DALTON
FULL PAPER

Generation of substrate-binding sites by electrochemical reduction of *cis*-$[Fe_2(cp)_2(\mu\text{-}SMe)_2(MeCN)(L)]^{2+}$ (L = CO or MeCN). Reactivity of the sites toward CO and ^{t}BuNC. Crystal structure of $[Fe_2(cp)_2(\mu\text{-}SMe)_2(CO)(MeCN)][BF_4]_2\cdot CH_2Cl_2$

Pascale Madec,[a] Kenneth W. Muir,[b] François Y. Pétillon,[a] René Rumin,[a] Yannick Scaon,[a] Philippe Schollhammer[a] and Jean Talarmin*[a]

[a] *UMR CNRS 6521 Chimie, Electrochimie Moléculaires et Chimie Analytique, Département de Chimie, Université de Bretagne Occidentale, 6 Av Le Gorgeu, BP809, 29285 Brest Cédex, France. E-mail: Jean.Talarmin@univ-brest.fr*
[b] *Department of Chemistry, University of Glasgow, UK G12 8QQ*

Received 8th April 1999, Accepted 3rd June 1999

Iron complexes with the $\{Fe_2(cp)_2(\mu\text{-}SMe)_2\}$ core have been synthesized and their electrochemistry investigated. Electrochemical reduction of the acetonitrile-substituted complexes *cis*-$[Fe_2(cp)_2(\mu\text{-}SMe)_2(MeCN)_2]^{2+}$ and *cis*-$[Fe_2(cp)_2(\mu\text{-}SMe)_2(CO)(MeCN)]^{2+}$ labilizes the MeCN ligand(s) and generates vacant sites at which CO and isocyanide substrates can bind. The mechanism of the electrochemical reduction of both complexes has been investigated in the presence of these substrates. A single-crystal X-ray analysis established that *cis*-$[Fe_2(cp)_2(\mu\text{-}SMe)_2(CO)(MeCN)][BF_4]_2$ contains an unusual dication in which different ligands (CO, MeCN) occupy corresponding sites in the co-ordination polyhedra of the two iron centres of the $Fe_2(\mu\text{-}S)_2$ ring. Aspects of the reactivity and electrochemistry of complexes with $Fe_2(\mu\text{-}SMe)_2$ and $Mo_2(\mu\text{-}SR)_2$ cores are compared.

Introduction

The chemistry of iron–sulfur compounds has received a great deal of attention because of the occurrence of Fe–S assemblies in various enzymes.[1] The wide area of abiological iron–sulfur complexes has also recently been reviewed.[2] Among synthetic Fe–S complexes, dinuclear cyclopentadienyl thiolate-bridged species have long been known.[3–17] Studies of isomerism in $[Fe_2(cp')_2(\mu\text{-}SR)_2(CO)_2]^{n+}$ complexes [cp′ = C_5H_5 (cp) or C_5Me_5 (cp*); R = alkyl or aryl, n = 0 or 1], of their redox and/or magnetic properties and of their crystal structures have appeared. However, their reactivity has been comparatively little explored.[10,12,16,17] In contrast, ruthenium analogues with a $\{Ru_2(cp^*)_2(\mu\text{-}SR)_n\}$ framework (n = 2 or 3)[18–20] are known to activate a variety of substrates (dihydrogen, alkyl halides, alkynes, hydrazines).[21–24]

The rich reactivity of $\{Ru_2(cp^*)_2(\mu\text{-}SR)_n\}$ complexes has prompted us to explore synthetic routes to the n = 2 iron(II) analogues[21,23,24] in order to gain access to chemistry at dinuclear, SR-bridged iron sites similar to that developed at ruthenium centres. We started our investigations with the bis(acetonitrile)iron(III) complex *cis*-$[Fe_2(cp)_2(\mu\text{-}SMe)_2(MeCN)_2]^{2+}$ originally synthesized by Kubas and Vergamini[16,17] because, in our studies of dinuclear molybdenum thiolate-bridged compounds,[25] we found that the lability of the acetonitrile ligands in $[Mo_2(cp)_2(\mu\text{-}SMe)_3(MeCN)_2]^+$ led to activation of hydrazines[26] and alkynes.[27] On the other hand, we have shown that M–NCMe bonds can electrochemically be cleaved to generate substrate-binding sites.[28,29] In the present paper we describe the electrochemical generation of co-ordination sites by reduction of the acetonitrile derivatives *cis*-$[Fe_2(cp)_2(\mu\text{-}SMe)_2(MeCN)_2]^{2+}$ and *cis*-$[Fe_2(cp)_2(\mu\text{-}SMe)_2(CO)(MeCN)]^{2+}$, as well as reactions of the sites with substrates. The X-ray analysis of crystals of the novel salt *cis*-$[Fe_2(cp)_2(\mu\text{-}SMe)_2(CO)(MeCN)][BF_4]_2\cdot CH_2Cl_2$ is also reported.

Results

The dicarbonyl complex $[Fe_2(cp)_2(\mu\text{-}SMe)_2(CO)_2]$ **1**, which was prepared as described previously,[8] is both the starting material for the syntheses of the acetonitrile-substituted dications and the product of their electrochemical reduction under CO (see below). The determination of the redox potentials of the two isomeric forms of the dicarbonyl complex, which would permit their ready identification by cyclic voltammetry, first requires each individual isomer to be differentiated. Two pairs of plausible *cis* and *trans* isomers[30] are shown.

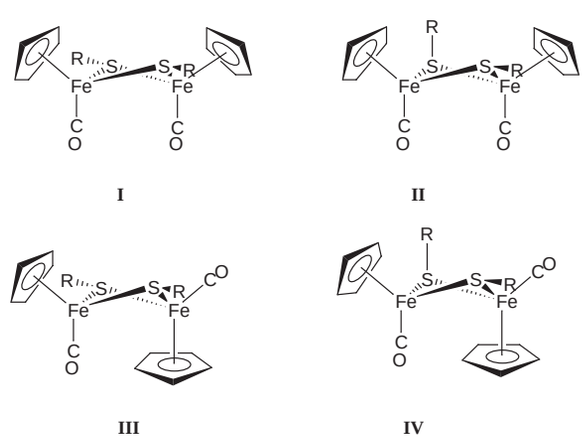

The isomers have been identified by variable temperature ^{1}H NMR spectroscopy in a manner similar to that used for their ruthenium[30] analogues. The *trans* isomer is fluxional; at low temperature the minor conformer is **III**, while the major conformer **IV** undergoes fast Fe_2S_2 ring inversion, even at 193 K. The values of the energy barriers for the **III** ↔ **IV** isomerisation, $\Delta G^{\ddagger}_{\mathbf{III}\longrightarrow\mathbf{IV}} = 59.3 \pm 1$ kJ mol^{-1}, and $\Delta G^{\ddagger}_{\mathbf{IV}\longrightarrow\mathbf{III}} = 61.0 \pm 1$ kJ mol^{-1}, have been estimated from the chemical shift difference, $\Delta\nu$, and from the coalescence temperatures of the cp or Me signals (T_c = 293 and 296 K, respectively).[31–33] These values are close to those determined for inversion of the sulfur atoms in the analogous ruthenium complexes.[30] The ^{1}H NMR spectrum of the *cis* isomer is not affected by temperature, but

Table 1 Redox potentials of the complexes in MeCN–$[NBu_4][PF_6]$ [a]

Complex	$E_{1/2}^{ox1}$	$E_{1/2}^{ox2}$	$E_{1/2}^{red1}$	$E_{1/2}^{red2}$
c-1 *cis*-$[Fe_2(cp)_2(\mu\text{-}SMe)_2(CO)_2]$	−0.48	0.08	−2.26 (irr)	
t-1 *trans*-$[Fe_2(cp)_2(\mu\text{-}SMe)_2(CO)_2]$	−0.42	0.19	−2.20 (irr)	
$\mathbf{2}^{2+}$ $[Fe_2(cp)_2(\mu\text{-}SMe)_2(MeCN)_2]^{2+}$			−0.64	−1.03 (irr)
				−1.15 (irr)
$\mathbf{3}^{2+}$ $[Fe_2(cp)_2(\mu\text{-}SMe)_2(CO)(MeCN)]^{2+}$			−0.27	−0.86 (irr) [b]
$[Fe_2(cp)_2(\mu\text{-}SMe)_2(CO)(Bu^tNC)]^{2+}$			−0.22	−0.85
$\mathbf{4}^{2+}$ *cis*-$[Fe_2(cp)_2(\mu\text{-}SMe)_2(Bu^tNC)_2]^{2+}$			−0.51	−1.20
$\mathbf{4}^{2+}$ *trans*-$[Fe_2(cp)_2(\mu\text{-}SMe)_2(Bu^tNC)_2]^{2+}$			−0.36	−1.04
5 $[Fe_2(cp)_2(\mu\text{-}SMe)_2(CN)_2]$	0.69		−1.18	−1.98

[a] Potentials (in V *vs.* Fc^+–Fc) were measured by cyclic voltammetry at a vitreous carbon electrode at a scan rate of 0.2 V s^{-1}. [b] The irreversible reduction of a product is detected at −2.0 V.

Table 2 NMR Data of the complexes [a]

Complex	^{1}H NMR (δ)	^{13}C NMR (δ)
$\mathbf{2}^{2+}$ $[Fe_2(cp)_2(\mu\text{-}SMe)_2(MeCN)_2]^{2+}$	5.62 (s, 10 H, C_5H_5)	140.8 (s, CN)
	2.47 (s, 6 H, SCH_3)	91.9 (s, C_5H_5)
	2.29 (s, 6 H, CH_3CN)	23.9 (s, SCH_3)
		4.3 (s, CH_3CN)
$\mathbf{3}^{2+}$ $[Fe_2(cp)_2(\mu\text{-}SMe)_2(CO)(MeCN)]^{2+}$	6.03 (s, 5 H, C_5H_5)	207.8 (s, CO)
	6.02 (s, 5 H, C_5H_5)	142.3 (s, CN)
	3.02 (s, 6 H, SCH_3)	95.6 (s, C_5H_5)
	2.29 (s, 3 H, CH_3CN)	34.2 (s, SCH_3)
		23.9 (s, SCH_3)
		4.4 (s, CH_3CN)
$\mathbf{4}^{2+}$ $[Fe_2(cp)_2(\mu\text{-}SMe)_2(Bu^tNC)_2]^{2+}$	5.82 (s, 10 H, C_5H_5)	142.8 (s, CN)
	2.88 (s, 6 H, SCH_3)	93.1 (s, C_5H_5)
	1.49 (s, 18 H, $(CH_3)_3C$)	62 (s, $(CH_3)_3C$)
		31 (s, SCH_3)
		30.5 (s, SCH_3)
		29.8 (s, $(CH_3)_3C$)
5 $[Fe_2(cp)_2(\mu\text{-}SMe)_2(CN)_2]$	5.04 (s, 10 H, C_5H_5) [b]	133.0 (s, CN) [b]
	2.51 (s, 6 H, SCH_3) [b]	88.9 (s, C_5H_5) [b]
		29.9 (s, SCH_3) [b]
$\mathbf{6}^{+}$ $[Fe_2(cp)_2(\mu\text{-}SMe)_3]^{+}$	5.57 (s, 10 H, C_5H_5)	87.5 (s, C_5H_5)
	3.01 (s, 3 H, SCH_3)	39 (s, SCH_3)
	2.83 (s, 3 H, SCH_3)	37 (s, SCH_3)
	0.08 (s, 3 H, SCH_3)	10 (s, SCH_3)

[a] NMR Spectra are recorded in $(CD_3)_2CO$ unless specified otherwise. [b] In $CDCl_3$.

fast Fe_2S_2 ring inversion cannot be ruled out. The *cis* isomer thus corresponds to **I** (equivalent cp and Me protons). In agreement with earlier results,[7,30] we observed that irradiation with uv light results in a *cis* to *trans* conversion, the reverse reaction being achieved thermally.

Since both isomers of $[Fe_2(cp)_2(\mu\text{-}SMe)_2(CO)_2]$ have thus unambiguously been identified, their redox potentials can be measured by cyclic voltammetry. Both complexes undergo two one-electron, diffusion-controlled oxidation steps which are reversible in MeCN and thf electrolytes and an irreversible reduction; we found the *cis* isomer easier to oxidize than the *trans* (Table 1), in agreement with previous results.[7]

Syntheses of *cis*-$[Fe_2(cp)_2(\mu\text{-}SMe)_2(L^1)(L^2)]^{n+}$ (L^1 = MeCN, L^2 = CO, MeCN, n = 2; L^1 = L^2 = ^{t}BuNC, n = 2; L^1 = L^2 = CN^-, n = 0)

Attempts to synthesize *cis*-$[Fe_2(cp)_2(\mu\text{-}SMe)_2(MeCN)_2]^{2+}$ $\mathbf{2}^{2+}$ from $[Fe_2(cp)_2(\mu\text{-}SMe)_2(CO)_2]$ by electrochemical methods were unsuccessful. However, the electrochemical synthesis of *cis*-$[Fe_2(cp)_2(\mu\text{-}SMe)_2(CO)(MeCN)]^{2+}$ $\mathbf{3}^{2+}$ met with limited success and produced variable, generally low (≤ 30%†) yields of the dication. The major product of the electrochemical oxidation was not characterized. Complex $\mathbf{2}^{2+}$ was eventually prepared from $[Fe_2(cp)_2(\mu\text{-}SMe)_2(CO)_2]$ by a modification of the procedure of Kubas and Vergamini.[16] It was characterized by comparing its ^{1}H NMR spectrum in CD_3CN with that of the original complex[16] (see Experimental section). Exchange of the MeCN ligands with the CD_3CN solvent is observed. Previously unreported ^{13}C NMR data are listed in Table 2.

$$\underset{\textbf{t-1}}{\textit{trans}\text{-}[Fe_2(cp)_2(\mu\text{-}SMe)_2(CO)_2]} \xrightarrow[\text{MeCN, 60 °C, 1 h}]{NO^+,\ O_2} \underset{\mathbf{3}^{2+}}{\textit{cis}\text{-}[Fe_2(cp)_2(\mu\text{-}SMe)_2(CO)(MeCN)]^{2+}} \quad (1)$$

The novel mono(acetonitrile) complex $\mathbf{3}^{2+}$ was obtained by oxidation of ***t*-1** with $NOBF_4$ in the presence of oxygen in MeCN [eqn. (1)]. The complex was characterized by microanalysis (experimental), ^{1}H and ^{13}C NMR spectroscopy (Table 2), and by a single crystal structure analysis (see below). It was obtained in at least 85% yield.

In order to characterize the products of the electrochemical reduction of complex $\mathbf{2}^{2+}$ in the presence of ^{t}BuNC and CN^-, the bis(isocyanide) and bis(cyanide) derivatives were prepared by treatment of $\mathbf{2}^{2+}$ with these substrates. The reaction with NaSMe was also examined (Scheme 1). Whereas $[Fe_2(cp)_2(\mu\text{-}SMe)_2(^tBuNC)_2]^{2+}$ $\mathbf{4}^{2+}$ and $[Fe_2(cp)_2(\mu\text{-}SMe)_3]^+$ $\mathbf{6}^+$ are novel, $[Fe_2(cp)_2(\mu\text{-}SMe)_2(CN)_2]$ **5** is the analogue of the previously

† The yields were estimated by cyclic voltammetry, from comparision of the peak current of the reactant to that of the product(s), assuming identical diffusion coefficients for both species.

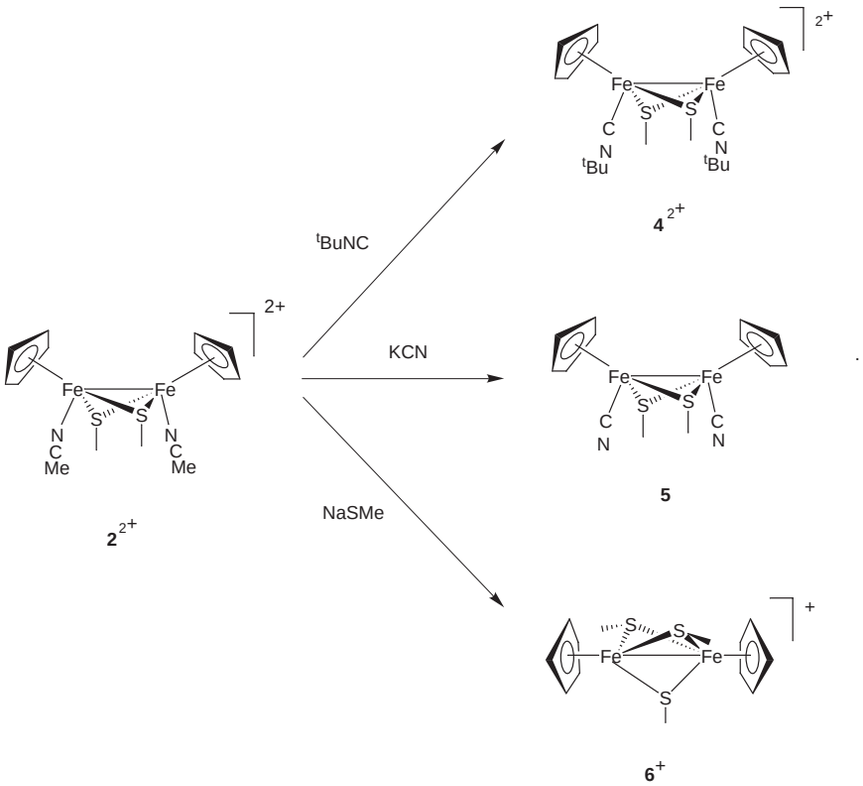

Scheme 1

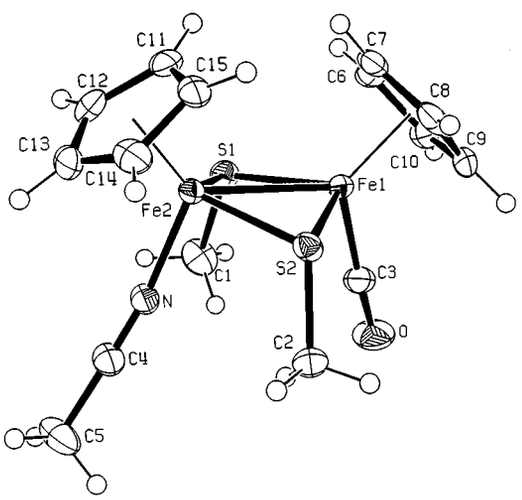

Fig. 1 A view of the dication in *cis*-$[Fe_2(cp)_2(\mu\text{-}SMe)_2(CO)(MeCN)][BF_4]_2\cdot CH_2Cl_2$ **3** showing 50% thermal ellipsoids for non-hydrogen atoms.

characterized ethanethiolate derivative.[17] The NMR data of $\mathbf{4}^{2+}$, **5**, and $\mathbf{6}^{+}$ are in Table 2. The ^{1}H and ^{13}C NMR spectra of $\mathbf{4}^{2+}$ are very similar to those of $\mathbf{2}^{2+}$ and show the equivalence of the cp ligands, of the SMe bridges and of the isocyanide groups. These data are consistent with a *cis* disposition of the cp rings and of the ^{t}BuNC ligands with respect to the Fe–Fe vector. A *syn* arrangement of the methyl substituents of the bridging sulfur atoms is also likely. The ^{13}C NMR spectrum of **5** is also in agreement with a *cis*-*syn* geometry for this complex. The ^{1}H and ^{13}C NMR spectra of **6** show the presence of two equivalent cp rings, and of three inequivalent SMe ligands, consistent with a $\{Fe_2(cp)_2(\mu\text{-}SMe)_3\}$ core.

Crystal structure of *cis*-$[Fe_2(cp)_2(\mu\text{-}SMe)_2(CO)(MeCN)][BF_4]_2\cdot CH_2Cl_2$ 3

Crystals of $[Fe_2(cp)_2(\mu\text{-}SMe)_2(CO)(MeCN)][BF_4]_2\cdot CH_2Cl_2$ contain discrete dinuclear $\mathbf{3}^{2+}$ dications, BF_4 anions and CH_2Cl_2 solvent molecules. A view of the dication is presented in Fig. 1 and pertinent bond distances and angles are listed in Table 3. Although several $[Fe_2(cp)_2(\mu\text{-}SR)_2(L^1)(L^2)]^{n+}$ complexes have now been crystallographically characterized (see Table 4), as far as we know $\mathbf{3}^{2+}$ is the first in which the ligands L^1 and L^2 are different. The cation contains (cp)Fe(CO) and (cp)Fe(NCMe) fragments bridged nearly symmetrically by two SMe ligands so that the co-ordination geometry about each iron atom is essentially that of a three-legged piano stool. The two cp rings are mutually *cis* with respect to the Fe–Fe bond and the CO and MeCN ligands occupy corresponding sites in the coordination

Table 3 Selected bond lengths (Å) and angles (°) in *cis*,*syn*-$[Fe_2(cp)_2(\mu\text{-}SMe)_2(CO)(MeCN)]^{2+}$ $\mathbf{3}^{2+}$

Fe1–Fe2	2.6555(6)	Fe2–N	1.924(3)
Fe1–C3	1.797(3)	Fe2–S1	2.2074(9)
Fe1–S1	2.2266(8)	Fe2–S2	2.2074(9)
Fe1–S2	2.2173(8)	Fe2–C11	2.097(3)
Fe1–C6	2.145(3)	Fe2–C12	2.130(3)
Fe1–C7	2.164(3)	Fe2–C13	2.141(3)
Fe1–C8	2.134(3)	Fe2–C14	2.106(3)
Fe1–C9	2.097(3)	Fe2–C15	2.088(3)
Fe1–C10	2.098(3)	S1–C1	1.809(4)
O–C3	1.126(4)	S2–C2	1.818(3)
N–C4	1.141(4)	C4–C5	1.456(5)
C3–Fe1–S1	92.46(11)	N–Fe2–S1	94.15(8)
C3–Fe1–S2	92.75(11)	N–Fe2–S2	91.65(8)
C3–Fe1–Fe2	108.98(10)	N–Fe1–Fe2	109.75(7)
S1–Fe1–S2	102.82(3)	S1–Fe2–S2	103.77(3)
S1–Fe1–Fe2	52.88(2)	S1–Fe2–Fe1	53.54(2)
S2–Fe1–Fe2	52.95(2)	S2–Fe2–Fe1	53.29(2)
S1–Fe1–Cp1	121.8(1)[a]	S1–Fe2–Cp2	120.8(1)[a]
S2–Fe1–Cp1	120.5(1)[a]	S2–Fe2–Cp2	120.6(1)[a]
C3–Fe1–Cp1	119.8(1)[a]	N–Fe2–Cp2	118.3(1)[a]
Fe1–S1–Fe2	73.58(3)	Fe1–S2–Fe2	73.76(3)
C1–S1–Fe1	114.42(13)	C2–S2–Fe1	113.09(13)
C1–S1–Fe2	111.86(12)	C2–S2–Fe2	113.40(12)
Fe1–C3–O	177.0(3)	Fe2–N–C4	168.7(3)
N–C4–C5	178.0(3)		

[a] Cp1 and Cp2 are the centroids of cp rings C6–C10 and C11–C15.

Table 4 Selected bond distances (Å) and angles (°) in the Fe_2S_2 core of *cis*-$[Fe_2(cp)_2(\mu\text{-}SR)_2(L^1)(L^2)]^{n+}$ complexes. Unless stated otherwise $L^1 = L^2 = CO$

Type	R	Fe–Fe	S–Fe–S	Fe–S–Fe	Ref.
(a) No Fe–Fe bond, $n = 0$					
	t-Bu	3.462(2)	80.1(1)	99.7(1)	4(*a*)
	t-Bu	3.461(2)	79.0(1)	98.9(1)	4(*a*)
	t-Bu	3.446(2)	78.9(1)	98.2(1)	4(*a*)
	Et	3.415(2)	81.1(1)	97.2(1)	14
	Et	3.450(2)	79.2(1)	99.1(1)	14
	Ph	3.39	81	98	4(*b*)
	$C_5H_9NMe_3$	3.438(1)	82.0(1)	97.9(1)	12
(b) 1e Fe–Fe bond, $n = +1$					
	Me	2.925(4)	95.4(1)	81.8(1)	5
	Ph	2.947	97.9	81.8	13
	Et	2.957(4)	95.7(2)	82.8(2)	11
(c) 2e Fe–Fe bond					
$L^1 = L^2 = MeCN$, $n = +2$	Et	2.649(7)	105.2(3)	73.9(3)	17
$L^1 = L^2 = CN$, $n = 0$	Et	2.625(3)	102.9(2)	73.3(2)	17
$L^1 = CO$, $L^2 = MeCN$, $n = +2$	Me	2.656(1)	103.8(1)	73.6(1)	This work
			102.8(1)	73.8(1)	

polyhedra of Fe1 and Fe2 [Cp1–Fe1–Fe2–Cp2 1.5(1); C3–Fe1–Fe2–N 2.0(1)°]. The centroids of the cp rings, Cp1 and Cp2, and the Fe1, Fe2, C3 and N atoms are coplanar to within ± 0.03 Å. This plane is a pseudo-mirror plane of symmetry in $\mathbf{3}^{2+}$, the distances of the S1 and S2 atoms from the plane being −1.75 and 1.72 Å respectively.

As in all the other compounds listed in Table 4 the methyl substituents of the bridging sulfur atoms in $\mathbf{3}^{2+}$ are *syn* and are situated on the same side of the slightly puckered Fe_2S_2 core as the CO and MeCN ligands. The dihedral angle between the two FeSFe planes [157.0(1)°] is close to that (156°) observed in the monocationic analogue, *cis*-$[Fe_2(cp)_2(\mu\text{-}SR)_2(CO)_2]^+$ where R = Me, though flatter rings are found in the monocations with R = Et (162) and Ph (172°).[5,11,13] The folding of the Fe_2S_2 ring in $\mathbf{3}^{2+}$ displaces the S atoms *away* from the cp rings so that the mean of the absolute values of the four C3– or N–Fe–Fe–S torsion angles is 78°. Corresponding values in the monocations with R = Et and Ph are 81 and 86°,[11,13] while in the molecular complexes listed in section (a) of Table 4 these angles are in the range 93–104°.

The Fe–Fe distance of 2.656(1) Å agrees well with comparable values for *cis*-$[Fe_2(cp)_2(\mu\text{-}SEt)_2(MeCN)_2]^{2+}$ and *cis*-$[Fe_2(cp)_2(\mu\text{-}SEt)_2(CN)_2]$ (see Table 4c); it falls in the 2.5–2.8 Å range which is characteristic of two-electron Fe–Fe bonds.[9,11] Longer Fe–Fe bond lengths are found in paramagnetic *cis*-$[Fe_2(cp)_2(\mu\text{-}SR)_2(CO)_2]^+$ cations for which a one-electron Fe–Fe bond is proposed;[5] this lengthening is accompanied by an increase (of *ca.* 8°) in the Fe–S–Fe angles (Table 4b). Still longer non-bonded Fe···Fe distances of 3.4 Å are found in the comparable iron(II) complexes and are accommodated by a further *ca.* 16° opening of the Fe–S–Fe angles to 97–100° (Table 4a).

In complex $\mathbf{3}^{2+}$ the Fe1–S bonds are longer than the Fe2–S bonds by 0.01–0.02 Å. The mean Fe–S bond distance [2.215 Å] is a little shorter than the values in paramagnetic *cis*-$[Fe_2(cp)_2(\mu\text{-}SR)_2(CO)_2]^+$ cations [2.234–2.251 Å]. Even larger mean Fe–S bond lengths of 2.267–2.281 Å accompany the long non-bonded Fe···Fe distances characteristic of *cis*-$[Fe^{II}_2(cp)_2(\mu\text{-}SR)_2(CO)_2]$ molecules.[4,5,11,12,17]

Electrochemical reduction of *cis*-$[Fe_2(cp)_2(\mu\text{-}SMe)_2(MeCN)_2]^{2+}$ and *cis*-$[Fe_2(cp)_2(\mu\text{-}SMe)_2(CO)(MeCN)]^{2+}$

The electrochemical reduction of the bis(acetonitrile) complex under a CO atmosphere involves the formation of the mixed CO/MeCN radical cation as an intermediate (see below). For sake of clarity, the electrochemical behaviour of *cis*-$[Fe_2(cp)_2(\mu\text{-}SMe)_2(CO)(MeCN)]^{2+}$ $\mathbf{3}^{2+}$ will be discussed first.

***cis*-$[Fe_2(cp)_2(\mu\text{-}SMe)_2(CO)(MeCN)]^{2+}$**. *In the absence of substrate.* Cyclic voltammetry (CV‡) of *cis*-$[Fe_2(cp)_2(\mu\text{-}SMe)_2(CO)(MeCN)]^{2+}$ $\mathbf{3}^{2+}$ in MeCN–$[NBu_4][PF_6]$ under an inert atmosphere shows that the complex undergoes three reduction steps [Fig. 2(a)]. The first ($E_{1/2}^{red1} = -0.27$ V) is a reversible, diffusion-controlled one-electron process whereas the second ($E_p^{red2} = -0.86$ V) is irreversible and produces a species detected by its irreversible reduction at $E_p^{red3} = -2.0$ V. Controlled-potential electrolysis at the potential of the first reduction produces the radical cation after consumption of 0.7 F per mol $\mathbf{3}^{2+}$. The complexes *cis*-$[Fe_2(cp)_2(\mu\text{-}SMe)_2(CO)_2]^{\bullet+}$ ($E_{1/2}^{red} = -0.48$ V; $E_{1/2}^{ox} = 0.08$ V) and *cis*-$[Fe_2(cp)_2(\mu\text{-}SMe)_2(MeCN)_2]^{2+}$ ($E_{1/2}^{red1} = -0.64$ V) were also present (10 to 20% †) in the catholyte [Fig. 2(b)]; the formation of these products along with the mixed CO/MeCN radical cation indicates that one-electron reduction of $\mathbf{3}^{2+}$ labilizes both the MeCN and CO ligands which can recombine with either of the co-ordinatively unsaturated sites to form the observed products (Scheme 2). The ligand exchange equilibria in Scheme 2 are responsible for the time-dependent distribution of the different complexes; the $\mathbf{2}^{2+}/\mathbf{3}^{\bullet+}$ ratio increases slightly when the solution is stirred under an inert atmosphere. Furthermore, the formation of the bis(acetonitrile) *dication* by reduction of $\mathbf{3}^{2+}$ accounts, at least in part, for the low *n* value ($n < 1$ F per mol $\mathbf{3}^{2+}$). Its formation from an electrogenerated radical cation must involve either an homogeneous redox reaction of *cis*-$[Fe_2(cp)_2(\mu\text{-}SMe)_2(MeCN)_2]^{\bullet+}$ $\mathbf{2}^{\bullet+}$with $\mathbf{3}^{2+}$, or the electrochemical *oxidation* of $\mathbf{2}^{\bullet+}$ according to an Electron Transfer Chain (ETC) catalysed process, at the potential of the controlled-potential *reduction* of $\mathbf{3}^{2+}$ (Scheme 2). Such a mechanism is reminiscent of the electrosynthesis of *cis*-$[Mo_2(cp)_2(\mu\text{-}SR)_2(CO)_3(MeCN)]^{2+}$ by electrochemical *reduction* of *cis*-$[Mo_2(cp)_2(\mu\text{-}SR)_2(CO)_4]^{2+}$ in MeCN.[31]

In the presence of a substrate (CO or ^{t}BuNC). As expected from the reactivity of the electrogenerated intermediates (Scheme 2), $\mathbf{3}^{\bullet+}$ reacts rapidly with CO to afford the dicarbonyl radical cation of *cis* geometry, ***c*-1**$^{\bullet+}$ [Fig. 2(c), Scheme 3]. Consistent with this, the first reduction of $\mathbf{3}^{2+}$ becomes less reversible in the presence of CO, and the reversible oxidation of ***c*-1**$^{\bullet+}$ is detected on the reverse scan [Fig. 3(a)]; the rate of the

‡ The parameters i_p and E_p are respectively the peak current and the peak potential of a redox process: $E_{1/2} = (E_p^a - E_p^c)/2$; E_p^a, i_p^a and E_p^c, i_p^c are respectively the potential and the current of the anodic and of the cathodic peak of a reversible process. An EC process comprises an electron transfer step (E) followed by a chemical reaction (C). rev = Reversible, irr = irreversible.

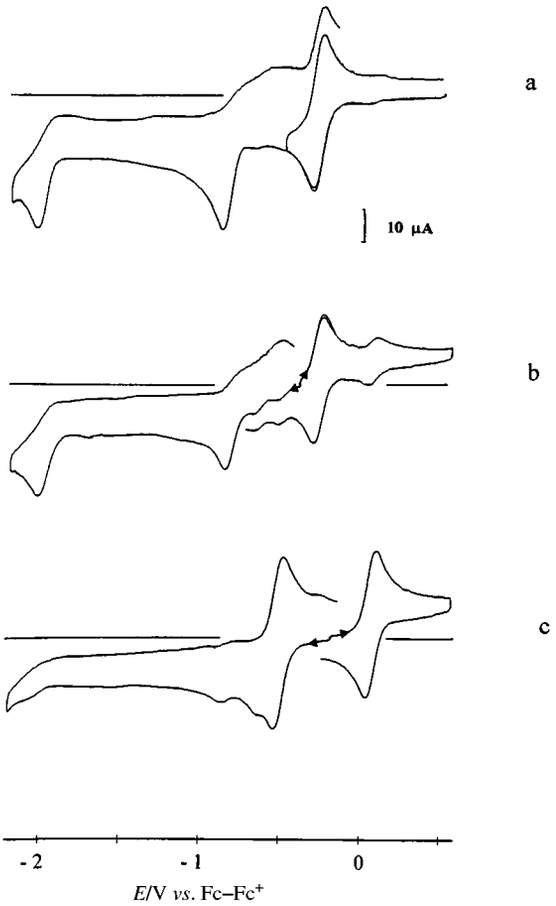

Fig. 2 Cyclic voltammetry of *cis*-$[Fe_2(cp)_2(\mu\text{-}SMe)_2(CO)(MeCN)]^{2+}$ $\mathbf{3}^{2+}$ (1.3 mM in MeCN–$[NBu_4][PF_6]$) (a) before and (b) after controlled-potential reduction at −0.37 V (platinum cathode, inert atmosphere, $n = 0.68$ F per mol $\mathbf{3}^{2+}$). The solution in (c) was obtained after treatment of that solution in (b) with CO (scan rate 0.2 V s^{-1}; vitreous carbon electrode).

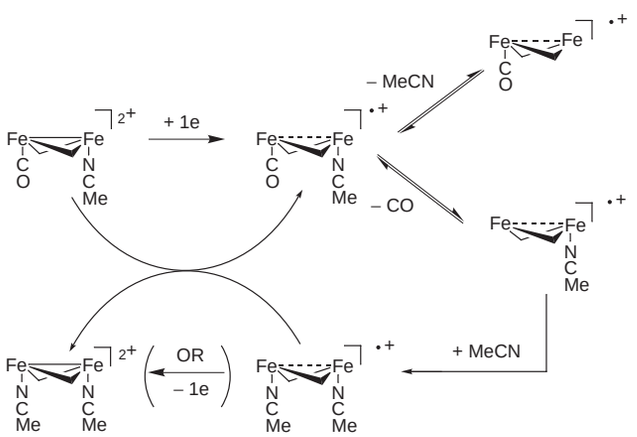

Scheme 2

chemical reaction following the electron transfer (EC process [35]) was estimated by cyclic voltammetry of $\mathbf{3}^{2+}$ under CO, from the scan rate dependence of the peak current ratio $[(i_p^a/i_p^c)^{red1}]$,[36,37] $k = 0.20 \pm 0.04$ s^{-1}. The reaction is slowed on lowering the temperature. At 253 K (1 atm CO) the formation of the *cis* dicarbonyl radical cation is not detected by CV ($v = 0.2$ V s^{-1}, switching potential −0.54 V). However, the oxidation of $\boldsymbol{c}$-$\mathbf{1}^{\bullet+}$ is observed on holding the potential at −0.54 V for a few seconds before scan reversal.

Treatment of $\mathbf{3}^{\bullet+}$ with ^{t}BuNC produces a complex with $E_{1/2}^{ox} = -0.22$ V, $E_{1/2}^{red} = -0.85$ V, assigned as *cis*-$[Fe_2(cp)_2(\mu\text{-}SMe)_2(CO)(^t BuNC)]^{\bullet+}$, by analogy with the formation of $\boldsymbol{c}$-$\mathbf{1}^{\bullet+}$ under CO. The rate constant of the chemical reaction could not be estimated from $(i_p^a/i_p^c)^{red1}$ measurements since $\mathbf{3}^{\bullet+}$ and *cis*-$[Fe_2(cp)_2(\mu\text{-}SMe)_2(CO)(^t BuNC)]^{\bullet+}$ oxidize reversibly at similar potentials ($E_{1/2}^{ox} = -0.27$ and −0.22 V, respectively). At low temperature (239 K) two reversible reduction steps are observed around −0.2 and −0.9 V, suggesting that substitution of MeCN by ^{t}BuNC in $\mathbf{3}^{\bullet+}$ still occurs.

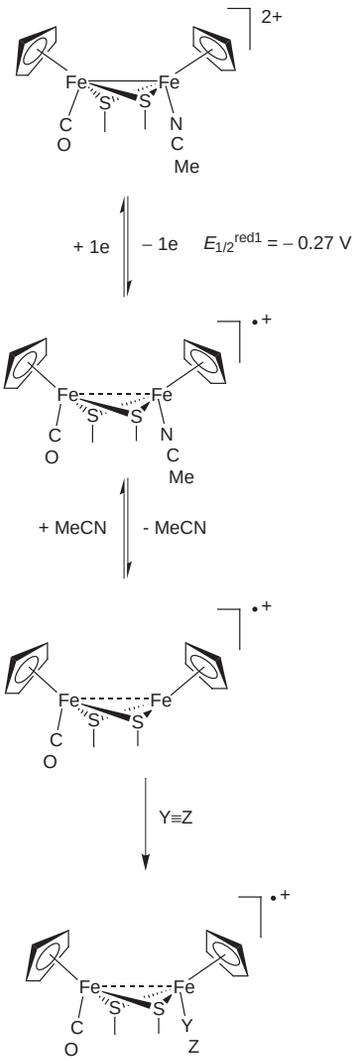

Scheme 3 Y≡Z = CO or ^{t}BuNC.

Controlled-potential electrolysis of complex $\mathbf{3}^{2+}$ at the potential of the first reduction in the presence of a substrate (Y≡Z = CO or ^{t}BuNC) produces *cis*-$[Fe_2(cp)_2(\mu\text{-}SMe)_2(CO)(Y{\equiv}Z)]^{\bullet+}$ almost quantitatively ($n = 0.7$–0.8 F per mol $\mathbf{3}^{2+}$). When Y≡Z = ^{t}BuNC, *cis*-$[Fe_2(cp)_2(\mu\text{-}SMe)_2(^t BuNC)_2]^{2+}$ $\mathbf{4}^{2+}$ is also present as a minor product (≤10%†). The disubstituted complex is likely to arise from the initial reaction of ^{t}BuNC with the $[Fe_2(cp)_2(\mu\text{-}SMe)_2(MeCN)]^{\bullet+}$ intermediate (Scheme 2, also see below).

When the potential scan includes the second reduction of $\mathbf{3}^{2+}$ (1 atm CO) both isomers of the neutral dicarbonyl complex, $\boldsymbol{c}$-**1** and $\boldsymbol{t}$-**1**, characterized by their distinct redox potentials, are detected on the return scan [Fig. 3(b)]. The formation of $\boldsymbol{t}$-**1** by reduction of a precursor in a *cis* geometry requires that an isomerization step is coupled to the electron transfer. The fact that reduction of $\mathbf{3}^{\bullet+}$ under CO produces *exclusively* the *trans* dicarbonyl was established as follows.

As indicated above, substitution of MeCN by CO in complex $\mathbf{3}^{\bullet+}$ is suppressed at low temperature $[(i_p^a/i_p^c)^{red1} \approx 1$, $v = 0.2$ V s^{-1}, $T = 253$ K, 1 atm CO]. Accordingly, the oxidation of $\boldsymbol{c}$-$\mathbf{1}^{\bullet+}$ is not observed by CV when the potential scan is reversed after

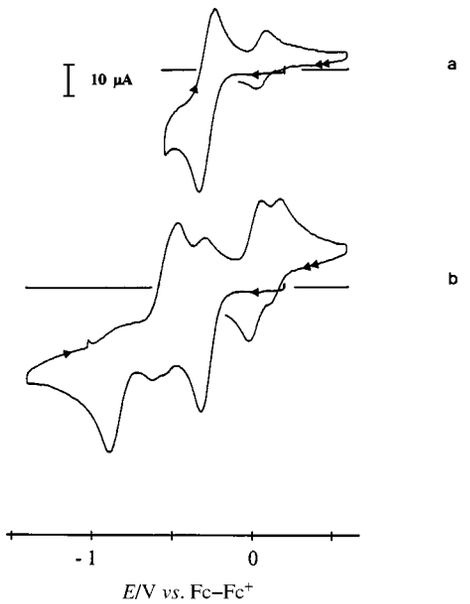

Fig. 3 Cyclic voltammetry of *cis*-$[Fe_2(cp)_2(\mu\text{-}SMe)_2(CO)(MeCN)]^{2+}$ $\mathbf{3}^{2+}$ (1.3 mM in MeCN–$[NBu_4][PF_6]$) under 1 atm CO (scan rate 0.2 V s^{-1}; vitreous carbon electrode).

the first reduction has been traversed. When the potential scan encompasses both reduction steps ***t*-1** is the only product detected (1 atm CO, $T = 236$ K). The facts that ***t*-1**$^{\bullet+}$ is not produced at the potential of the first reduction, and that ***c*-1** is not detected in the low temperature CV, make it clear that the second reduction of $\mathbf{3}^{2+}$ in the presence of CO affords *only* ***t*-1**. If the structure change was subsequent to the electron transfer and to the release of MeCN, then one would expect *cis*-$[Fe_2(cp)_2(\mu\text{-}SMe)_2(CO)_2]$ to be the major product, or at least to be one of the products, depending on the relative rates of the isomerization and of CO binding at the vacant site. The fact that only ***t*-1** is formed at low temperature indicates that the isomerisation is concerted with the second reduction of $\mathbf{3}^{2+}$ (Scheme 4); it appears likely that the structure change is allowed

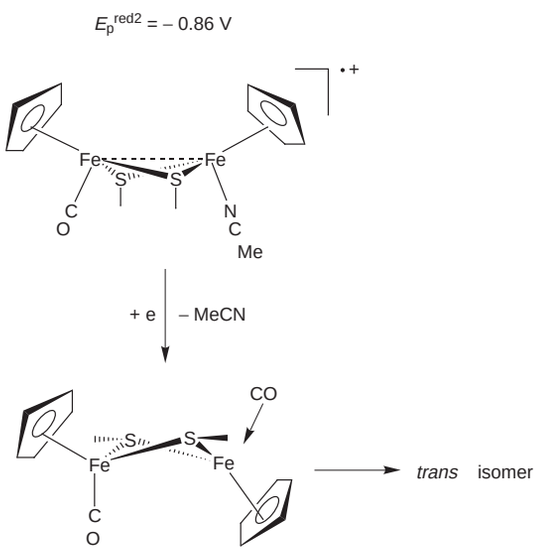

Scheme 4

by cleavage of the Fe–Fe bond after transfer of two electrons. It has been shown that the presence of a metal–metal bond in $\{Rh_2(\mu\text{-}SR)_2(L)_2\}$ complexes prevents inversion of the Rh_2S_2 ring whereas this process takes place ($\Delta G^{\ddagger} = 38$–44 kJ mol^{-1}) in the absence of such a bond.[38,39]

From the above results it can also be concluded that the irreversible reduction observed at $E_p^{red} = -2.0$ V in the absence

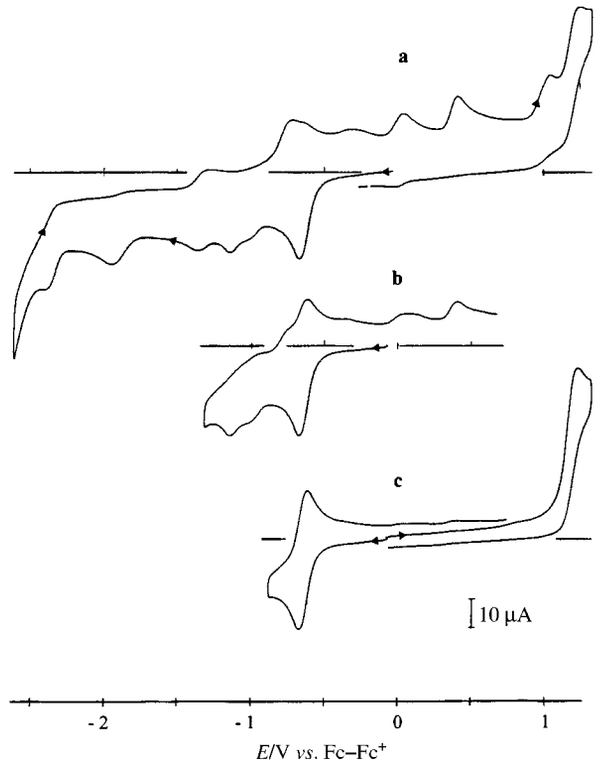

Fig. 4 Cyclic voltammetry of *cis*-$[Fe_2(cp)_2(\mu\text{-}SMe)_2(MeCN)_2]^{2+}$ $\mathbf{2}^{2+}$ in MeCN–$[NBu_4][PF_6]$ under an inert atmosphere (scan rate 0.2 V s^{-1}; vitreous carbon electrode).

of substrate [Fig. 2(a)], and suppressed in the presence of CO or ^{t}BuNC, arises from the reduction of the co-ordinatively unsaturated Fe^{II}_2 species $[Fe_2(cp)_2(\mu\text{-}SMe)_2(CO)]$.

***cis*-$[Fe_2(cp)_2(\mu\text{-}SMe)_2(MeCN)_2]^{2+}$.** *In the absence of substrate.* Cyclic voltammetry of complex $\mathbf{2}^{2+}$ in MeCN–$[NBu_4][PF_6]$ under an inert atmosphere shows several reduction peaks in the potential range from 0 to -2.5 V *vs.* Fc^+–Fc, [Fig. 4(*a*)]. The reduction steps between -1.5 and -2.5 V, and the irreversible, multi-electron oxidation of the complex [Fig. 4(c)] will not be discussed here. The first reduction at $E_{1/2}^{red1} = -0.64$ V [Fig. 4(c)] is a diffusion-controlled one-electron step ($\Delta E_p^{red1} \approx 60$ mV, $i_p^{red1}/v^{1/2}$ independent of scan rate, v, for $0.02 \leq v \leq 1$ V s^{-1});‡ this reduction is not completely reversible as indicated by a slight increase of the anodic to cathodic peak current ratio with increasing scan rates [$(i_p^a/i_p^c)^{red1} = 0.8$ at $v = 0.02$ V s^{-1}; 1.0 at $v = 0.15$ V s^{-1}]. The reduction peaks at $E_p^{red} = -1.03$ and -1.15 V [Fig. 4(b)] are assigned to products generated by the first reduction (EC process[35]) on the basis of low temperature cyclic voltammetry: under these conditions where the first reduction appears fully reversible [$(i_p^a/i_p^c)^{red1} = 1$], the redox processes at -1.03 and -1.15 V are absent. Instead, a new irreversible peak due to the second reduction of $\mathbf{2}^{2+}$ is observed at -1.4 V. The fact that the first reduction of $\mathbf{2}^{2+}$ is irreversible in thf–$[NBu_4][PF_6]$ strongly suggests that the chemical step coupled to the electron transfer is the de-co-ordination of a MeCN ligand. Whereas this reaction is irreversible in thf, it occurs according to a fast equilibrium in MeCN. This is similar to the reactivity of $\mathbf{3}^{\bullet+}$ described above.

The low temperature experiment (MeCN electrolyte), the CV in Fig. 4(b) and 4(c), and the electrochemical behaviour of complex $\mathbf{2}^{2+}$ in a thf electrolyte can be rationalized by the reactions shown in Scheme 5. The radical cation $\mathbf{2}^{\bullet+}$ is connected to the co-ordinatively unsaturated site, $[Fe_2(cp)_2(\mu\text{-}SMe)_2(MeCN)]^{\bullet+}$, by a fast equilibrium. This equilibrium is shifted towards $\mathbf{2}^{\bullet+}$ by its oxidation to $\mathbf{2}^{2+}$ [*cf.* $(i_p^a/i_p^c)^{red1} \approx 1$ in Fig. 4(c)], and toward $[Fe_2(cp)_2(\mu\text{-}SMe)_2(MeCN)]^{\bullet+}$ by its irreversible reduction around -1.1 V [*cf.* $(i_p^{red2}/i_p^{red1}) \approx 0.4$ in

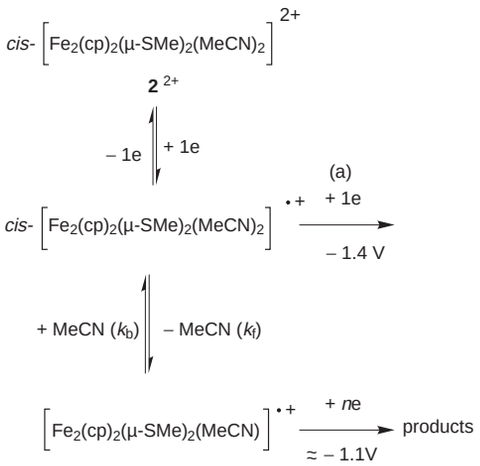

Scheme 5 (a) At low temperature in MeCN–$[NBu_4][PF_6]$.

Fig. 4(b)]. The absence of the latter at low temperature suggests that MeCN de-co-ordination is prevented. However, in the presence of a substrate Y≡Z, formation of substituted derivatives is observed (see below, Y≡Z = CO or ^{t}BuNC). Therefore, $[Fe_2(cp)_2(\mu\text{-}SMe)_2(MeCN)]^{\bullet+}$ can still be produced at low temperature; it is likely that temperature affects the rate constants k_f and k_b differently (Scheme 5) so that, at low temperature in the absence of substrate, the equilibrium favours $\mathbf{2}^{\bullet+}$.

The reduction products of $[Fe_2(cp)_2(\mu\text{-}SMe)_2(MeCN)]^{\bullet+}$ are detected by oxidation steps on the reverse scan at −0.78 (reversible), 0 and around 0.4 V [in MeCN, $E_p^{ox} = 0.45$ V (irr); thf, $E_{1/2}^{ox} = 0.35$ V (rev); Fig. 4(a) and 4(b)] and by irreversible reduction peaks between −1.5 and −2.5 V [Fig. 4(a)]. One is tentatively assigned as $[Fe_2(cp)_2(\mu\text{-}SMe)_3]$ since $[Fe_2(cp)_2(\mu\text{-}SMe)_3]^+$ $\mathbf{6}^+$ undergoes a reversible reduction at −0.78 V, and an oxidation which is irreversible in MeCN ($E_p^{ox} = 0.45$ V) and reversible in thf ($E_{1/2}^{ox} = 0.33$ V). Formation of the tris(thiolate)-bridged radical by reduction of $[Fe_2(cp)_2(\mu\text{-}SMe)_2(MeCN)]^{\bullet+}$ would indicate that the $\{Fe^{II}{}_2\}$ complex $[Fe_2(cp)_2(\mu\text{-}SMe)_2]$ which might have formed is unstable under our experimental conditions and is stabilized by co-ordination of a SMe radical; insertion of a SR radical in the metal–metal bond of $[Rh_2(cp)_2(\mu\text{-}SR)_2]^{\bullet+}$ has also been observed.[39] In contrast to the apparent lack of stability of $[Fe_2(cp)_2(\mu\text{-}SMe)_2]$, the $[Ru_2(cp^*)_2(\mu\text{-}SR)_2]$ analogue could be crystallographically characterized (R = $C_6H_3Me_2$-2,6).[40] While loss of the MeCN ligand preceding co-ordination of SMe is the most probable route to $[Fe_2(cp)_2(\mu\text{-}SMe)_3]$, the reverse reaction order is also possible. It has been shown that $[M_2(cp')_2(\mu\text{-}SR)_3]$ reacts with CO and isocyanide to produce $[(SR)(cp')M(\mu\text{-}SR)_2M(cp')(Y{\equiv}Z)]$ for M = Ru (Y≡Z = CO or BuNC; cp′ = cp*).[18] It is conceivable that in the case where M = Fe and YZ = MeCN (cp′ = cp) such a species would rearrange to $[Fe_2(cp)_2(\mu\text{-}SMe)_3]$. The reactions leading to this complex by reduction of $[Fe_2(cp)_2(\mu\text{-}SMe)_2(MeCN)]^{\bullet+}$ are an example of deactivation[28,29] that a substrate-binding site may undergo when generated in the absence of a suitable substrate.

Under CO. In MeCN–$[NBu_4][PF_6]$ the presence of CO causes substantial changes in the CV of complex $\mathbf{2}^{2+}$. The first reduction becomes irreversible and its potential is shifted positively by *ca.* 80 mV compared to that under N_2 or Ar. The reduction peaks around −1.1 V are absent, replaced by an irreversible process at $E_p^{red2} = -0.86$ V. Furthermore, all the reduction peaks detected between −1.5 and −2.5 V under N_2 or Ar are suppressed. The irreversible reduction of $[Fe_2(cp)_2(\mu\text{-}SMe)_2(CO)_2]$ **1** is present around −2.2 V. The scan rate dependence of the peak current ratio i_p^{red2}/i_p^{red1} demonstrates that the irreversible step at −0.86 V is due to the reduction of a product formed at the first reduction, namely *cis*-$[Fe_2(cp)_2(\mu\text{-}SMe)_2(CO)(MeCN)]^{\bullet+}$ $\mathbf{3}^{\bullet+}$. This is entirely consistent with the binding of CO at the vacant site generated by the one-electron reduction

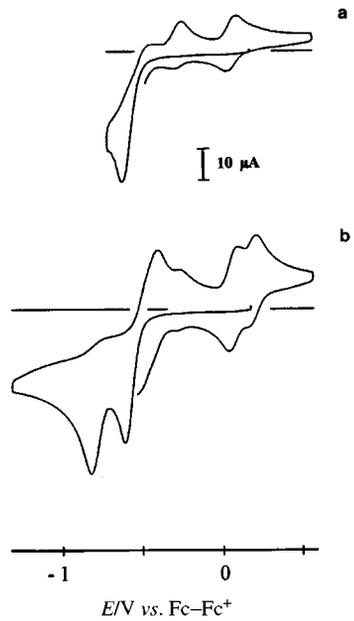

Fig. 5 Cyclic voltammetry of *cis*-$[Fe_2(cp)_2(\mu\text{-}SMe)_2(MeCN)_2]^{2+}$ $\mathbf{2}^{2+}$ in MeCN-$[NBu_4][PF_6]$ under CO (1 atm) showing (a) the formation of the *cis* dicarbonyl and (b) the formation of *cis*- and *trans*-$[Fe_2(cp)_2(\mu\text{-}SMe)_2(CO)_2]$ when the potential range includes both reduction steps (scan rate 0.2 V s^{-1}; vitreous carbon electrode).

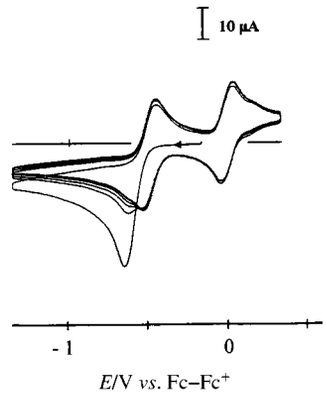

Fig. 6 Repetitive scan cyclic voltammetry of *cis*-$[Fe_2(cp)_2(\mu\text{-}SMe)_2(MeCN)_2]^{2+}$ $\mathbf{2}^{2+}$ in thf–$[NBu_4][PF_6]$ under CO (1 atm) (scan rate 0.2 V s^{-1}; vitreous carbon electrode).

of $\mathbf{2}^{2+}$ (Scheme 5) and with the potential of the second reduction of $\mathbf{3}^{2+}$ (see above).

The plot of the current function for the first reduction, $i_p^{red1}/v^{1/2}$, against the scan rate, v, deviates markedly from linearity at slow scan rates, indicating the occurrence of an ECE mechanism[35] under CO. The rate constant of the intervening chemical step ($k = 0.3 \pm 0.1$ s^{-1}) was estimated by CV, from the ratio of the current functions measured in the presence and in the absence of CO, $F_c^{red1}(k)/F_c^{red1}(d)$.[41] The intermediate and the product of the ECE process are detected on the reverse scan by their oxidation [$E_{1/2}^{ox} = -0.27$ and 0.08 V, respectively; Fig. 5(a)]. When both reduction steps are included in the potential scan [Fig. 5(b)] both *cis* and *trans* isomers of **1** are formed, in agreement with the above results. Low temperature CV demonstrates that CO binding to *cis*-$[Fe_2(cp)_2(\mu\text{-}SMe)_2(MeCN)]^{\bullet+}$ still takes place, and confirms that the substitution of MeCN by CO in *cis*-$[Fe_2(cp)_2(\mu\text{-}SMe)_2(CO)(MeCN)]^{\bullet+}$ is suppressed under these conditions (see above).

Cyclic voltammetry of complex $\mathbf{2}^{2+}$ in thf–$[NBu_4][PF_6]$ provides further information about the reduction mechanism. Under a CO atmosphere the first reduction of $\mathbf{2}^{2+}$ is an irreversible two-electron process in the thf electrolyte (Fig. 6). The redox steps of the mixed CO/MeCN intermediate are not

observed which demonstrates that the substitution of the second MeCN ligand by CO is fast in thf, whereas this is the slow step of the reduction process in MeCN. This is consistent with the occurrence of an equilibrium in this solvent. Furthermore, the dicarbonyl product is present essentially as the *cis* isomer, in agreement with the fact that the *trans* analogue resulted exclusively from the reduction of *cis*-$[Fe_2(cp)_2(\mu\text{-}SMe)_2(CO)(MeCN)]^{\bullet+}$.

The slow step of the ECE reduction of complex $\mathbf{2}^{2+}$ in MeCN–$[NBu_4][PF_6]$ under CO is the same as that of the EC reduction of $\mathbf{3}^{2+}$ under the same conditions, *i.e.* substitution of the MeCN ligand by CO in *cis*-$[Fe_2(cp)_2(\mu\text{-}SMe)_2(CO)(MeCN)]^{\bullet+}$. The two estimates of the rate constant of this reaction, $k = 0.3 \pm 0.1$ and $0.20 \pm 0.04\ s^{-1}$ (ECE and EC mechanisms, respectively) are in modest agreement and can only be used to determine an approximate value, $k \approx 0.25\ s^{-1}$ (MeCN–$[NBu_4][PF_6]$).

The overall reduction mechanism of complex $\mathbf{2}^{2+}$ at the potential of the first reduction under CO in MeCN–$[NBu_4][PF_6]$ is presented in Scheme 6. This mechanism is also valid in a thf electrolyte except that the substitution of the second acetonitrile ligand is at least as fast as the first one.

In the presence of ^{t}*BuNC.* Although treatment of complex $\mathbf{2}^{2+}$ with ^{t}BuNC produces the bis(isocyanide) derivative $\mathbf{4}^{2+}$ (see above and Experimental section), the thermal process does not take place to a significant extent on the timescale of the electrochemical experiment; the bis(acetonitrile) complex is still the species present in the bulk of the solution after addition of ^{t}BuNC as demonstrated by the fact that the irreversible oxidation of $\mathbf{2}^{2+}$ is detected on the first positive-going potential scan. The CV of $\mathbf{2}^{2+}$ in MeCN–$[NBu_4][PF_6]$ is significantly affected by the presence of ^{t}BuNC (2 equivalents) however. The first reduction of $\mathbf{2}^{2+}$ is shifted positively by *ca.* 100 mV, and a second, reversible one-electron reduction process is present at $E_{1/2}^{red2} = -1.20$ V; the reduction steps between -1.5 and -2.5 V are absent. The presence of the reduction at $E_{1/2}^{red2} = -1.20$ V, due to the *cis*-$[Fe_2(cp)_2(\mu\text{-}SMe)_2(^tBuNC)_2]^{\bullet+/0}$ couple, arises from the formation of the bis(isocyanide) radical cation in the electrode vicinity when the potential scan reaches the reduction potential of $\mathbf{2}^{2+}$ (EC process[35]). The chemical (substrate-binding) steps of the EC process are not suppressed at low temperature (233 K, MeCN–$[NBu_4][PF_6]$), the reduction at $E_{1/2}^{red2} = -1.20$ V still being observed under these conditions. No mixed ^{t}BuNC/MeCN product is detected by CV ($v \leq 1$ V s^{-1}), indicating that the binding of the second ^{t}BuNC ligand at the radical cation stage is at least as fast as binding of the first one.

Controlled-potential electrolysis at the potential of the first reduction of complex $\mathbf{2}^{2+}$ in the presence of ^{t}BuNC (2 equivalents) affords the bis(isocyanide) radical cation, characterized by its redox potentials (Table 1), essentially quantitatively after consumption of *ca.* 0.7 F per mol $\mathbf{2}^{2+}$, Fig. 7(a). The reduction mechanism of $\mathbf{2}^{2+}$ in the presence of ^{t}BuNC is likely to be similar to that shown in Scheme 6 (replacing CO by ^{t}BuNC) except for the rate of the second MeCN susbstitution. In the present case, the electrochemical reduction of $\mathbf{2}^{2+}$ at -0.7 V does not occur according to an ECE mechanism, since the reduction of *cis*-$[Fe_2(cp)_2(\mu\text{-}SMe)_2(^tBuNC)_2]^{\bullet+}$ $\mathbf{4}^{\bullet+}$ takes place at -1.20 V, a potential about 0.5 V more negative than the electrolysis potential. The neutral complex can be generated electrochemically however. Controlled-potential reduction of the radical cation at -1.4 V ($n = 0.9$ F per mol $\mathbf{4}^{\bullet+}$) affords two products assigned as *cis*- and *trans*-$[Fe_2(cp)_2(\mu\text{-}SMe)_2(^tBuNC)_2]$ [Fig. 7(b), Table 1], by analogy with the formation of ***t*-1** by reduction of $\mathbf{3}^{\bullet+}$ under CO (see above). The isomerization step, which is again facilitated by cleavage of the Fe–Fe bond, is likely to relieve steric strain caused by the bulky ^{t}BuNC ligands in a *cis* position.

In the presence of cyanide. In contrast with the above examples where the presence of the substrate affected only the CV of complex $\mathbf{2}^{2+}$, addition of cyanide leads to the rapid

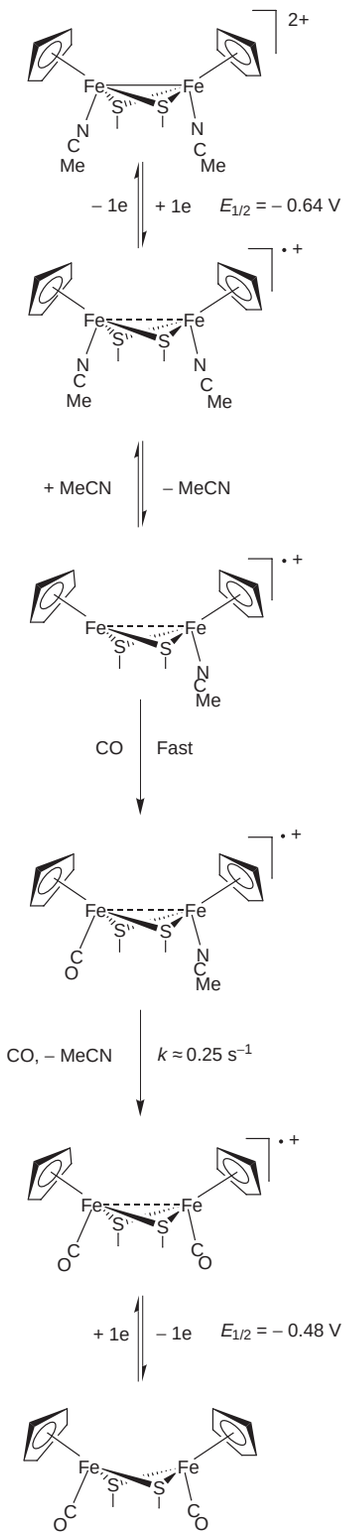

Scheme 6

formation of *cis*-$[Fe_2(cp)_2(\mu\text{-}SMe)_2(CN)_2]$ **5**, on the timescale of the electrochemical experiment: the solution instantly turns from orange to blue-green on addition of CN^- and *all* the redox features of $\mathbf{2}^{2+}$ are replaced by those of **5** after addition of 2 equivalents cyanide.

Monitoring by CV of the stepwise addition of $[NBu_4][CN]$ (0–2 equivalents) to a solution of complex $\mathbf{2}^{2+}$ in MeCN–$[NBu_4][PF_6]$ shows that the first reduction ($E_{1/2}^{red1} = -0.64$ V) decreases steadily on addition of cyanide whereas a reduction peak at $E_p^{red} = -1.02$ V first increases (0–1 equivalent CN^-) and then decays (1–2 equivalents CN^-). The latter is attributed

to $[Fe_2(cp)_2(\mu\text{-}SMe)_2(CN)(MeCN)]^+$. The detection of the mixed CN/MeCN intermediate indicates that substitution of the second MeCN ligand by cyanide is slower than the first one. The reduction peak of the final product **5** ($E_{1/2}^{red1} = -1.18$ V) is maximum after addition of 2 equivalents CN^-. Complex **5** is also characterized by a second irreversible reduction ($E_p^{red2} = -1.98$ V) and by a reversible one-electron oxidation ($E_{1/2}^{ox} = 0.69$ V).

Discussion

Reactivity of the Fe^{III}–Fe^{III} and of the $Fe^{III} \cdots Fe^{II}$ sites with substrates

The reactivity of the $\{Fe_2(cp)_2(\mu\text{-}SMe)_2^{2+}\}$ site [formally $\{Fe^{III}$–$Fe^{III}\}$] can be summarized as follows: (i) in MeCN the CO groups of complex $\mathbf{1}^{2+}$ can be successively replaced by solvent molecules to afford $\mathbf{3}^{2+}$ and $\mathbf{2}^{2+}$; (ii) the MeCN ligands of $\mathbf{2}^{2+}$ are labile (MeCN/CD_3CN exchange is observed by ^1H NMR in CD_3CN), and are thermally substituted by ^{t}BuNC, even in neat MeCN, in a slow reaction; (iii) cyanide and methanethiolate anions react rapidly with $\mathbf{2}^{2+}$ to produce complexes **5** and $\mathbf{6}^+$. From these observations it appears that the preferred ligands at the $\{Fe^{III}$–$Fe^{III}\}$ site follow the order $CN^- > {}^t$BuNC > MeCN > CO. Except for the inversion of the MeCN/ ^{t}BuNC couple, this corresponds to decreasing electron-releasing ability of the different ligands L, as deduced from the first reduction potential of *cis*-$[Fe_2(cp)_2(\mu\text{-}SMe)_2(L)_2]^{n+}$ ($n = 0$ or 2; Table 1). Owing to the different nature of $[Fe_2(cp)_2(\mu\text{-}SMe)_3]^+$, the thiolate anion was not included in the above series.

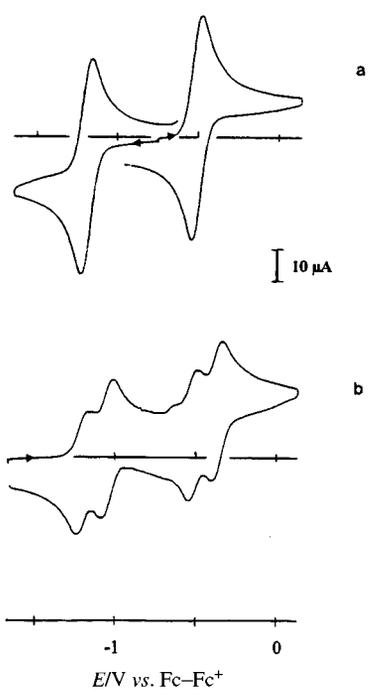

Fig. 7 Cyclic voltammetry of the catholyte after (a) controlled-potential reduction of *cis*-$[Fe_2(cp)_2(\mu\text{-}SMe)_2(MeCN)_2]^{2+}$ $\mathbf{2}^{2+}$ (1 mM) at −0.7 V in the presence of 2 equivalents ^{t}BuNC (platinum cathode, inert atmosphere, $n = 0.70$ F per mol $\mathbf{2}^{2+}$), and (b) after reduction of the solution in (a) at −1.45 V (platinum cathode, inert atmosphere, $n = 0.91$ F per mol $\mathbf{2}^{2+}$) (MeCN–$[NBu_4][PF_6]$; scan rate 0.2 V s^{-1}; vitreous carbon electrode).

The complex *cis*-$[Fe_2(cp)_2(\mu\text{-}SMe)_2(MeCN)_2]^{2+}$ $\mathbf{2}^{2+}$ is the precursor of different radical cations. A characteristic of the radical cations with MeCN and/or CO ligands is the lability of these groups. First, one-electron reduction of $\mathbf{2}^{2+}$ leads to de-co-ordination of one MeCN ligand. This reaction is irreversible in thf, and reversible in MeCN where the equilibrium is quite mobile. Carbon monoxide and ^{t}BuNC can also bind at the unsaturated $[Fe_2(cp)_2(\mu\text{-}SMe)_2(MeCN)]^{\bullet+}$ site. Secondly, in *cis*-$[Fe_2(cp)_2(\mu\text{-}SMe)_2(CO)(MeCN)]^{\bullet+}$, CO and MeCN are released in reversible steps. Comparison of the reactions of (i) a given site with different substrates and (ii) different sites with a common substrate, at room and at low temperatures, allows a qualitative picture of site reactivities to be drawn. The reactions taken into account on the basis of the results described above are illustrated in Scheme 7. The equilibria may be shifted to either side depending on the electronic properties of the ligand L and of the substrate Y≡Z.

The reaction of complex $\mathbf{3}^{\bullet+}$ with CO (Scheme 7, L = Y≡Z = CO) is suppressed at low temperature, while that with Y≡Z = ^{t}BuNC is not. Therefore, ^{t}BuNC is a better ligand than CO for the particular site concerned; this suggests that the steric bulk of the incoming nucleophile is not critical to binding which appears to be mainly governed by the electronic properties of the substrate. At low temperature, CO co-ordination is slowed sufficiently for competition between CO and MeCN for the vacant site (Scheme 7, steps c and b) to turn in favour of the solvent, MeCN.

On the other hand, temperature changes do not induce this 'on/off' effect on the reaction of CO with complex $\mathbf{2}^{\bullet+}$ (Scheme 7, L = MeCN, Y≡Z = CO), since the reaction still takes place at low temperature. Clearly, in $[(L)(cp)Fe(cp)(\mu\text{-}SMe)_2Fe(cp)(MeCN)]^{\bullet+}$ the acetonitrile ligand is more labile for L = MeCN (in $\mathbf{2}^{\bullet+}$) than for CO (in $\mathbf{3}^{\bullet+}$) which indicates that L affects the reactivity of the neighbouring Fe atom, *i.e.* the occurrence of a bimetallic effect.

The reduction of complex $\mathbf{3}^{\bullet+}$ and $[Fe_2(cp)_2(\mu\text{-}SMe)_2(MeCN)]^{\bullet+}$ causes a further increase of the net electron density on the dinuclear framework. This was anticipated to produce co-ordinatively unsaturated $\{Fe^{II}_2\}$ sites. However, we have shown that the electrochemical reduction of $[Fe_2(cp)_2(\mu\text{-}SMe)_2(MeCN)]^{\bullet+}$ leads to decomposition; $[Fe_2(cp)_2(\mu\text{-}SMe)_3]$ is a probable deactivation product of $[Fe_2(cp)_2(\mu\text{-}SMe)_2]$, which thus appears to be much less stable than the $[Ru_2(cp^*)_2(\mu\text{-}SR)_2]$ analogues.[40]

Comparison of dinuclear thiolate-bridged carbonyl complexes of Fe and Mo

We have previously investigated the effects of ligands (C_5R_5 rings, sulfur substituents) and of metal centres (V, Mo, W) on the reactivity and electrochemical behaviour of isostructural and isoelectronic dinuclear cyclopentadienyl thiolate-bridged complexes.[25] The present study provides the opportunity to compare iron and molybdenum derivatives.

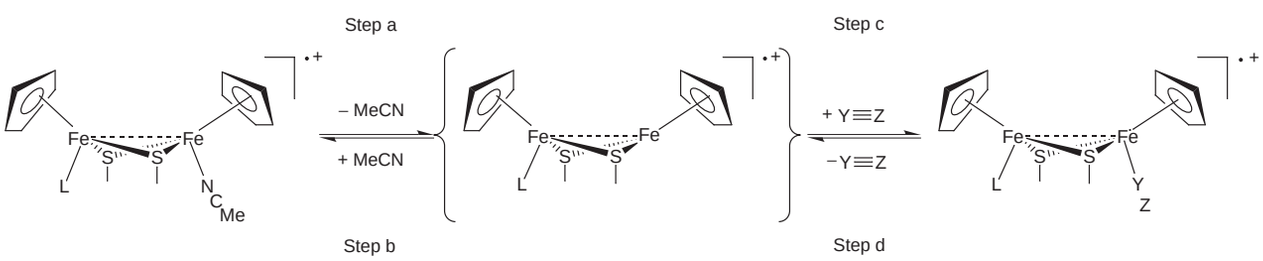

Scheme 7

Redox chemistry of $[M_2(cp)_2(\mu\text{-}SMe)_2(CO)_n]$ and the associated structure change. The metal centres of the M^{II}_2 carbonyl complexes $[M_2(cp)_2(\mu\text{-}SMe)_2(CO)_n]$ ($n = 2$, M = Fe or Mo; $n = 4$, M = Mo) have a closed-shell configuration; the two-electron difference between d^6 iron and d^4 molybdenum in these species is formally compensated in the molybdenum complexes by the presence of a supplementary (2e-donor) CO ligand on each metal centre ($n = 4$) or by a metal–metal double bond ($n = 2$). The presence of a metal–metal (double) bond only in $[Mo_2(cp)_2(\mu\text{-}SMe)_2(CO)_2]$, and the nature of the orbitals associated with the Mo=Mo bond, might be the reason why the molybdenum dicarbonyl behaves quite differently from the other two complexes; for example, $[Mo_2(cp)_2(\mu\text{-}SMe)_2(CO)_2]$ undergoes two reversible one-electron reductions and an irreversible multi-electron oxidation,[42] while $[Fe_2(cp)_2(\mu\text{-}SMe)_2(CO)_2]$ and $[Mo_2(cp)_2(\mu\text{-}SMe)_2(CO)_4]$ can be reversibly oxidized to the dication, and are cleaved on reduction.

Structural characterization of molybdenum compounds (neutral[43,44] and dication[45]) and of iron complexes (neutral,[4,12,14,15] radical cations[5,11,13,15] and dications;[17] also see above and Tables 3 and 4) clearly illustrates a substantial deformation of the M_2S_2 core due to the formation of a M–M bond upon oxidation. This is due to the $\sigma^*_{M\text{-}M}$ character of the highest occupied molecular orbital (HOMO) of the neutral molybdenum[46] and iron[5,47] complexes.§ The decrease of the M-M separation on one-electron oxidation destabilizes the metal–metal antibonding singly occupied molecular orbital (SOMO) of the radical cation,[46] which should favour the transfer of a second electron at the same potential as the first. Accordingly, both **1** and *cis*-$[Mo_2(cp)_2(\mu\text{-}SMe)_2(CO)_4]$ could be expected to oxidize in an overall two-electron step; however, this is true only for the molybdenum complex.[45] At this point, it is interesting that the reduction of *cis*-$[Mo_2(cp^*)_2(\mu\text{-}SMe)_2(CO)_4]^{2+}$ occurs according to an overall two-electron process in thf and MeCN electrolytes [$E_{1/2}^{red} = -0.65$ V ($\Delta E_p = 40$ mV) and $E_{1/2}^{red} = -0.63$ V ($\Delta E_p = 35$ mV), respectively] whereas two overlapping one-electron couples are observed in CH_2Cl_2 with $E_{1/2}^{red1} = -0.62$ V ($\Delta E_p = 64$ mV) and $E_{1/2}^{red2} = -0.69$ V ($\Delta E_p = 66$ mV).[28b] In contrast, the second oxidation of *cis*-$[Fe_2(cp)_2(\mu\text{-}SMe)_2(CO)_2]$ occurs at a potential well positive of $E_{1/2}^{ox1}$ (*cis*, $\Delta E_{1/2}^{ox} = 0.56$ V; *trans*, $\Delta E_{1/2}^{ox} = 0.61$ V), indicating that, while *cis*-$[Mo_2(cp)_2(\mu\text{-}SMe)_2(CO)_4]^{\bullet+}$ has no thermodynamic stability, the iron radical cation is quite stable thermodynamically (*cis*, $K_{comp} = 3.1 \times 10^9$; *trans*, $K_{comp} = 2.2 \times 10^{10}$).

Furthermore, despite the amount of structural reorganization involved (Table 4), the cyclic voltammetric peak-to-peak separation (ΔE_p) for both oxidation couples of complex **1** (both isomers, $v = 0.2$ V s^{-1}) is close to that expected for reversible systems [$\Delta E_p = (58/n)$ mV at 298K]. Electron-transfer steps coupled to structural changes are generally characterized by ΔE_p larger than that for the reversible case, because the energy required for rearranging (bond making and/or breaking, changes in bond angles) contributes to the energy barrier to electron transfer.[48,49] Detailed investigations[50] of the electrochemistry of **1**, *cis*-$[Fe_2(cp)_2(\mu\text{-}PPh_2)_2(CO)_2]$ and $[Mo_2(cp)_2(\mu\text{-}SMe)_4]$ in different solvents and at different electrodes have shown that the standard heterogeneous electron-transfer rates of the iron compounds, which both undergo substantial structure change upon oxidation, are almost as large as that of the molybdenum derivative whose structure is little affected by oxidation.[51] Since the inner-sphere reorganization energy appears to contribute little to the activation barrier to electron transfer for these iron complexes, the authors suggested that the electron transfer and the structure change may not be actually kinetically coupled.[50]

§ The first oxidation of both *cis*-$[M_2(cp)_2(\mu\text{-}SMe)_2(CO)_n]$ complexes occurs at similar potentials [M = Fe ($n = 2$): $E_{1/2}^{ox1} = -0.48$ V; M = Mo ($n = 4$): $E_{1/2}^{ox} = -0.54$ V[45]], suggesting that the energies of their (HOMO) are similar.

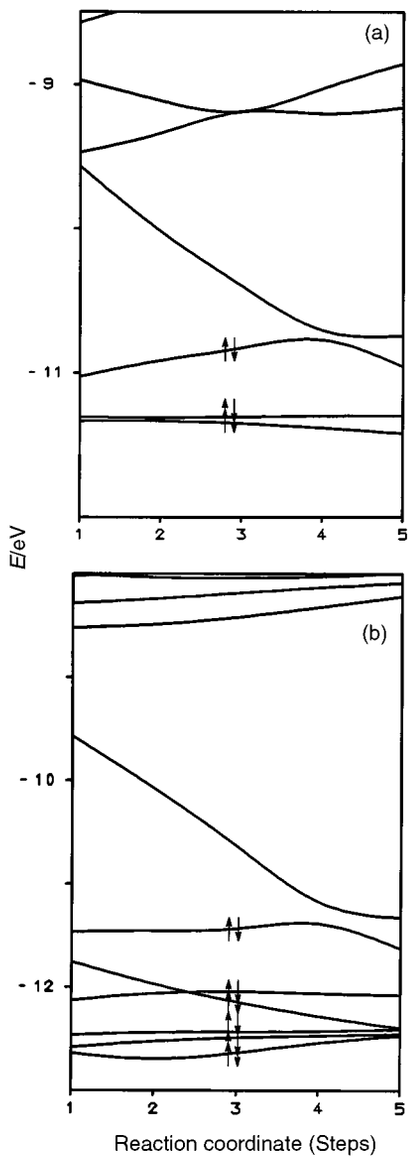

Fig. 8 Walsh diagrams associated with the variations of the M_2S_2 core dimensions (M–M, M–S, S···S distances, M–S–M, S–M–S angles, angle between two M–S–M planes) and of the M–C(O) bonds length on going from *cis*-$[M_2(cp)_2(\mu\text{-}SMe)_2(CO)_n]^{2+}$ to *cis*-$[M_2(cp)_2(\mu\text{-}SMe)_2(CO)_n]$. (a) M = Mo, $n = 4$; (b) M = Fe, $n = 2$.

The electronic structure of *cis*-$[Mo_2(cp)_2(\mu\text{-}SR)_2(CO)_4]^{2+/0}$ [46] and of $[M_2(\mu\text{-}X)_2(CO)_8]$ [47] complexes have been studied using the extended Hückel method. The LUMO of the molybdenum dication is made of a metal–metal hybrid ($d_{yz} + d_{z^2}$: 31%) with the four CO π^* orbitals (45% total) mixing in a bonding fashion to the metal orbitals. In order to try to rationalize the different redox behaviour of *cis*-$[M_2(cp)_2(\mu\text{-}SMe)_2(CO)_n]^{2+/0}$ (M = Mo, $n = 4$; M = Fe, $n = 2$), we have studied by EHMO calculations the frontier orbital changes resulting from M_2S_2 ring deformations for both species. The model complexes, *cis*-$[Mo_2(cp)_2(\mu\text{-}SH)_2(CO)_4]^{2+}$ and *cis*-$[Fe_2(cp)_2(\mu\text{-}SH)_2(CO)_2]^{2+}$, were constructed using the X-ray crystallographic data of *cis*-$[Mo_2(cp)_2(\mu\text{-}S^tBu)_2(CO)_4]^{2+}$ [45] and of *cis*-$[Fe_2(cp)_2(\mu\text{-}SEt)_2(MeCN)_2]^{2+}$ [17] and *cis*-$[Fe_2(cp)_2(\mu\text{-}SMe)_2(CO)(MeCN)]^{2+}$ (Table 3), respectively. The LUMO of the iron dication is associated with the Fe_2S_2 core and contains metal–metal (57%) and metal–sulfur (26%) antibonding characters. The net overlap population between the metal centres in the dication [0.101 (Mo); 0.119 (Fe)] is in agreement with the presence of a M–M bond, while the M–M overlap population in the LUMO [−0.084 (Mo); −0.191 (Fe)] is consistent with cleavage of the M–M bond upon reduction. Deformation of the M_2S_2 core

from the dimensions assumed in the dication [step 1, Fig. 8(a) and (b)] to those of the neutral complex [step 5, Fig. 8(a) and (b)] effectively results in an extensive stabilization of the LUMO, so that an avoided crossing of the frontier orbitals is eventually observed for both complexes. Comparison of the Walsh diagrams shows one difference between the molybdenum and iron derivatives. From Fig. 8(a) (step 1) it can be seen that one-electron reduction of the molybdenum dication would result in a radical cation having a small HOMO/LUMO gap (*ca.* 0.13 eV) if no structure change was involved; this may trigger the rearrangement which provides a larger separation of the frontier orbitals. On the contrary, the radical cation produced by one-electron reduction of the iron dication could be stable, even without rearranging, with a HOMO/LUMO separation of *ca.* 1 eV [Fig. 8(b), step 1]; it is conceivable that the structural change may be slower in this case, which might give support to the suggestion that the rearrangement is not kinetically coupled to the electron-transfer step.[50]

EHMO Calculations of the electronic structure of the iron dication and radical cation models allow an estimation of the energy stabilization of the LUMO (ΔE_1) resulting from the first reduction of *cis*-$[Fe_2(cp)_2(\mu\text{-}SH)_2(CO)_2]^{2+}$ and the associated structure change, $\Delta E_1 \approx 0.85$ eV. On the contrary, the molybdenum radical cation is not stable so that its structure (geometric and electronic) is unknown. The only safe conclusion which can be drawn in this case is that the stabilization of the LUMO due to the *first* electron transfer-induced rearrangement is $\Delta E \leq \Delta E_{1+2}$, *i.e. ca.* 1.2 eV ($\Delta E_{1+2}$ is the stabilization of the LUMO resulting from the transfer of 2 electrons). One reason for the different redox behaviour of the iron and molybdenum complexes might be that the stabilization of the LUMO resulting from the *first electron transfer* (ΔE_1) is large enough to overcome the spin pairing energy in the case of the molybdenum dication, thus allowing the transfer of a second electron at E^{red1}, whereas it is insufficient in the case of Fe.

Substitution reactions in *cis*-$[M_2(cp)_2(\mu\text{-}SMe)_2(CO)_n]^{2+/\bullet+}$ and electrochemistry of *cis*-$[M_2(cp)_2(\mu\text{-}SMe)_2(CO)_{n-1}(MeCN)]^{2+}$. The reactivity of $[Mo_2(cp)_2(\mu\text{-}SMe)_2(CO)_2]$ is different from that of the other M^{II}_2 complexes, $[Fe_2(cp)_2(\mu\text{-}SMe)_2(CO)_2]$ and $[Mo_2(cp)_2(\mu\text{-}SR)_2(CO)_4]$ (R = Me or Ph), in that substitution of one CO by isocyanide is easy.[42] For the latter two complexes substitution requires oxidation of the molecule. As indicated above, substitution of MeCN for CO in **1** under electrochemical activation was found to produce little *cis*-$[Fe_2(cp)_2(\mu\text{-}SMe)_2(CO)(MeCN)]^{2+}$, but this compound was obtained in >85% yield by chemical oxidation of **1** in MeCN at 333 K. Similarly, *cis*-$[Mo_2(cp)_2(\mu\text{-}SR)_2(CO)_3(MeCN)]^{2+}$ was obtainable by heating *cis*-$[Mo_2(cp)_2(\mu\text{-}SR)_2(CO)_4]^{2+}$ in neat acetonitrile,[52] whereas the cp* analogue was not.[28b] Both compounds could be prepared electrochemically by oxidation of $[Mo_2(cp')_2(\mu\text{-}SR)_2(CO)_4]$ or by reduction of the corresponding dication in MeCN–$[NBu_4][PF_6]$ at 313 K.[28b,34] The electrochemical route was found to be the only access[28b,52] to the isocyanide complexes *cis*-$[Mo_2(cp')_2(\mu\text{-}SR)_2(CO)_3(RNC)]^{2+/0}$.

The electrochemical reduction of *cis*-$[Mo_2(cp)_2(\mu\text{-}SMe)_2(CO)_3(MeCN)]^{2+}$ is an irreversible two-electron process leading to loss of the acetonitrile ligand.[28a] On the other hand, two discrete one-electron reduction steps are observed for the cp* analogue and reversible de-co-ordination of the MeCN ligand at the radical cation stage could be evidenced.[28b] The site generated by MeCN loss can bind CO and RNC substrates[28] which makes the reactivity of *cis*-$[Mo_2(cp')_2(\mu\text{-}SMe)_2(CO)_3(MeCN)]^{2+}$ (cp′ = cp or cp*) and that of *cis*-$[Fe_2(cp)_2(\mu\text{-}SMe)_2(CO)(MeCN)]^{2+}$ similar in this respect.

Conclusion

The results presented in this paper show that the electrochemical reduction of MeCN-substituted diiron complexes leads to the generation of reactive binding sites. However, under our experimental conditions, it proved impossible to form $[Fe_2(cp)_2(\mu\text{-}SMe)_2]$, with a vacant site at each metal centre, by electrochemical reduction of *cis*-$[Fe_2(cp)_2(\mu\text{-}SMe)_2(MeCN)_2]^{2+}$. Complexes with η^2-co-ordinated Y–Z substrates, which are among the objectives of our work, might still be accessible by stepwise co-ordination of the substrate upon reduction of the bis-acetonitrile dication. This possibility will be examined.

Comparison of dinuclear molybdenum and iron thiolate-bridged complexes showed that $[Mo_2(cp)_2(\mu\text{-}SMe)_2(CO)_2]$ has a quite different redox chemistry and reactivity compared to those of the iron dicarbonyl. This is assigned to the occurrence of a metal–metal double bond in the molybdenum complex. In contrast, *cis*-$[Mo_2(cp)_2(\mu\text{-}SMe)_2(CO)_4]^{0/2+}$ and the MeCN-substituted dication *cis*-$[Mo_2(cp)_2(\mu\text{-}SMe)_2(CO)_3(MeCN)]^{2+}$ present similarities with $[Fe_2(cp)_2(\mu\text{-}SMe)_2(CO)_2]^{0/2+}$ and *cis*-$[Fe_2(cp)_2(\mu\text{-}SMe)_2(CO)(MeCN)]^{2+}$, respectively. Therefore, the formal compensation of two d electrons by a supplementary 2e ligand on each Mo atom rather than by a Mo=Mo double bond results in complexes whose properties are closer to those of the iron derivatives $[Fe_2(cp)_2(\mu\text{-}SMe)_2(CO)(L)]^{n+}$ (L = CO, $n = 0$ or 2; L = MeCN, $n = 2$) despite more different geometry and co-ordination number. Although a substantial structure change is associated with the electron transfer steps for both *cis*-$[M_2(cp)_2(\mu\text{-}SMe)_2(CO)_n]^{0/2+}$ (M = Mo, $n = 4$; M = Fe, $n = 2$), the nature of the overall redox process is different: the iron complex undergoes two successive, reversible one-electron transfers while the molybdenum complex oxidizes (/ reduces) in a reversible two-electron step. A possible explanation of this difference has been proposed.

Experimental

Methods and materials

Unless specified otherwise, all the experiments were carried out under an inert atmosphere, using Schlenk techniques for the syntheses. Tetrahydrofuran (thf) was purified as described previously.[53] Acetonitrile (Carlo Erba or BDH, HPLC grade) was used as received. The preparation and the purification of the supporting electrolyte $[NBu_4][PF_6]$ and the electrochemical equipment were as described previously.[53] All the potentials (text, tables, figures) are quoted against the ferrocenium–ferrocene couple; ferrocene was added as an internal standard at the end of the experiments. The ^1H and ^{13}C NMR spectra were recorded on a Bruker AC300 spectrometer.

MO calculations

All the MO calculations were of the extended Hückel type[54] using the weighted H_{ij} formula.[55] The atomic parameters were taken from the literature.[56] Calculations were made with the CACAO package developed by Mealli and Proserpio.[57]

Syntheses

***cis*-$[Fe_2(cp)_2(\mu\text{-}SMe)_2(MeCN)_2][PF_6]_2$ $2[PF_6]_2$.** The complex was obtained following a procedure similar to that described previously,[16] slightly modified in order to convert *cis*-$[Fe_2(cp)_2(\mu\text{-}SMe)_2(CO)_2]$ into the *trans* isomer. A solution of $[Fe_2(cp)_2(\mu\text{-}SMe)_2(CO)_2]$ (2.6 g, 6.6 mmol; *cis* + *trans* isomers) and NH_4PF_6 (4 g, 24.5 mmol) in 200 mL acetonitrile was irradiated (Philips HPK 125W) for 1.5 h and stirred at room temperature in the air for 3 d. The solution was filtered to eliminate a brown precipitate. The filtrate was taken to dryness and the residue washed twice with 100 mL water and twice with 75 mL CH_2Cl_2. The product was dried under vacuum (yield: 1.57 g, 33%) ^{1}H NMR (CD_3CN): δ 5.33 (s, 10 H, C_5H_5), 2.25 (s, 6 H, SCH_3) and 2.07 (s, CH_3CN) [compare with ref. 16: 5.38 (s, C_5H_5), 2.26 (s, SCH_3), 2.07 (s, CH_3CN)].

***cis*-[$Fe_2(cp)_2(\mu\text{-}SMe)_2(CO)(MeCN)][BF_4]_2$ 3[$BF_4]_2$.** A solution of *trans*-[$Fe_2(cp)_2(\mu\text{-}SMe)_2(CO)_2$] (1 g, 2.55 mmol) and [NO][BF_4] (0.895 g, 3 equivalents) in 30 mL CH_3CN was heated at 60 °C for 1 h under an oxygen stream. The solution was then taken to dryness and the residue washed with dichloromethane and recrystallized in an acetone–dichloromethane mixture (yield: 1.28 g, 87%). Calc. for $C_{15}H_{19}B_2F_8Fe_2NOS_2$: C, 31.1; H, 3.3; N, 2.4. Found: C, 29.9; H, 3.5; N, 2.4%.

[$Fe_2(cp)_2(\mu\text{-}SMe)_2(^tBuNC)_2][PF_6]_2$ 4[$PF_6]_2$. A solution of [$Fe_2(cp)_2(\mu\text{-}SMe)_2(MeCN)_2][PF_6]_2$ (0.132 g, 0.186 mmol) and ^{t}BuNC (210 μL, 10 equivalents) in 100 mL MeCN was stirred for 2 d at room temperature under an inert atmosphere. The solvent was evaporated under vacuum and the residue washed with CH_2Cl_2. The solution was filtered and the solid was dried under vacuum (yield: 0.10 g, 68%). Calc. for $C_{11}H_{17}FeF_6NPS$: C, 33.3; H, 4.3; N, 3.5. Found: C, 33.6; H, 4.6; N, 3.4%.

***cis*-[$Fe_2(cp)_2(\mu\text{-}SMe)_2(CN)_2$] 5.** To a solution of [$Fe_2(cp)_2(\mu\text{-}SMe)_2(MeCN)_2][PF_6]_2$ (0.20 g, 0.28 mmol) in 10 mL MeCN was added KCN (0.092 g, 1.41 mmol) dissolved in the minimum water. The solution was stirred for 5–10 min under an inert atmosphere. The solvent was evaporated and the residue extracted several times with CH_2Cl_2 (150 mL total). The brown-orange solution was taken to dryness and the solid dried under vacuum (yield: 0.087 g, 80%). Calc. for C_7H_8FeNS: C, 43.3; H, 4.2; N, 7.2. Found: C, 43.7; H, 4.3; N, 7.1%.

[$Fe_2(cp)_2(\mu\text{-}SMe)_3][PF_6]$ 6[PF_6]. To a solution of 0.10 g (0.14 mmol) of [$Fe_2(cp)_2(\mu\text{-}SMe)_2(MeCN)_2][PF_6]_2$ in 5mL MeCN was added 1 equivalent (0.010 g) NaSMe. The solution was stirred at room temperature for 10 min. The solvent was removed under vacuum and the residue stirred with 10 mL acetone. The solution was filtered and the filtrate taken to dryness. The residue was chromatographed on a silica gel column; [$Fe_2(cp)_2(\mu\text{-}SMe)_3][PF_6]$ was eluted with a CH_2Cl_2–acetone 9 : 1 mixture. The solution was taken to dryness and the solid dried under vacuum. Yield 0.052 g, 70%. Calc. for $C_{13}H_{19}F_6Fe_2PS_3$: C, 29.6; H, 3.6; Fe, 21.2; P, 5.9. Found: C, 30.8; H, 3.8; Fe, 21.9; P, 5.7%.

X-Ray analysis of [$Fe_2(cp)_2(\mu\text{-}SMe)_2(CO)(MeCN)$] [$BF_4]_2 \cdot CH_2Cl_2$ 3

Several attempts to measure the diffraction data using conventional X-ray sources failed because the crystals were too small. Eventually, measurements were made successfully at 150 K on a Bruker-SMART CCD diffractometer using synchrotron radiation, $\lambda = 0.69150$ Å, and a red micro-crystal of dimensions 0.10 × 0.06 × 0.06 mm.

Crystal data. $C_{15}H_{19}B_2F_8Fe_2NOS_2 \cdot CH_2Cl_2$, $M = 663.68$, orthorhombic, space group $P2_12_12_1$, $a = 10.770(1)$, $b = 11.683(1)$, $c = 19.751(2)$ Å, $V = 2485.0(4)$ Å^3, $Z = 4$, $F(000) = 1328$, $D_c = 1.774$ Mg m^{-3}, $\mu = 1.62$ mm^{-1}.

The intensities of 14 544 reflections with $2 < \theta(\text{Mo-K}\alpha) < 27°$ were corrected for Lorentz-polarization effects and absorption (empirical correction factors 1.000–0.768).[58] Averaging gave 5283 unique reflections ($R_{int} = 0.033$); for 4971 of these $I > 2\sigma(I)$. The structure was solved by Patterson methods; 311 parameters were refined on F^2 to $R1 = 0.035$ and $wR_2 = 0.087$ for all 5283 data. In the final difference map $|\Delta\rho| < 0.78$ e Å^{-3}. Anisotropic U_{ij} were refined for all non-hydrogen atoms. Hydrogen atoms rode on parent C atoms and an orientation parameter was refined for each methyl group. The absolute structure was established by experiment [Flack parameter 0.02(2)]. Scattering factors and dispersion corrections were those incorporated in the least-squares refinement program SHELXL 97 and the WINGX package was used for other calculations.[59,60]

CCDC reference number 186/1488.

See http://www.rsc.org/suppdata/dt/1999/2371/ for crystallographic files in .cif format.

Acknowledgements

We thank Centre National de la Recherche Scientifique (France), EPSRC (UK), UBO (Université de Bretagne Occidentale) and Glasgow University for financial support. K. W. M. also thanks Drs. David Taylor and Simon Coles for their help in collecting data.

References

1 R. H. Holm, P. Kennepohl and E. I. Solomon, *Chem. Rev.*, 1996, **96**, 2239.
2 H. Ogino, S. Inomata and H. Tobita, *Chem. Rev.*, 1998, **98**, 2093.
3 R. B. King and M. B. Bisnette, *Inorg. Chem.*, 1965, **4**, 482.
4 (*a*) B. I. Kolobkov, S. E. Nefedov, I. L. Eremenko, A. A. Pasynskii, A. I. Yanovskii and Yu. T. Struchkov, *Zh. Neorg. Khim.*, 1992, **37**, 328; (*b*) G. Ferguson, C. Hannaway and K. M. S. Islam, *Chem. Commun.*, 1968, 1165.
5 N. G. Connelly and L. F. Dahl, *J. Am. Chem. Soc.*, 1970, **92**, 7472.
6 M. Chase, H. A. O. Hill, C. E. Johnson and R. Richards, *Chem. Commun.*, 1970, 1376.
7 J. A. de Beer, R. J. Haines, R. Greatrex and J. A. van Wyk, *J. Chem. Soc., Dalton Trans.*, 1973, 2341.
8 J. A. de Beer, R. J. Haines and R. Greatrex, *J. Organomet. Chem.*, 1975, **85**, 89.
9 P. D. Frisch, M. K. Lloyd, J. A. McCleverty and D. Seddon, *J. Chem. Soc., Dalton Trans.*, 1973, 2268.
10 D. D. Watkins and T. A. George, *J. Organomet. Chem.*, 1975, **102**, 71.
11 R. B. English, *Acta Crystallogr., Sect. C*, 1984, **40**, 1567.
12 W. Gaete, J. Ros, R. Yanez, X. Solans and M. Font-Altaba, *J. Organomet. Chem.*, 1986, **316**, 169.
13 A. A. Pasynskii, I. L. Eremenko, M. A. Porai-Koshits, S. B. Katser, A. S. Antsyshkina, A. S. Katugin, B. Orazsakhatov, O. Y. Okhlobystin and V. I. Privalov, *Metalloorg. Khim.*, 1990, **3**, 454.
14 M. T. Toshev, Kh. B. Dustov, A. I. Nekhaev, G. G. Aleksandrov, S. D. Alekseeva and B. I. Kolobkov, *Koord. Khim.*, 1991, **17**, 930.
15 R. Büchner, J. S. Field and R. J. Haines, *J. Chem. Soc., Dalton Trans.*, 1996, 3533; 1997, 2403.
16 G. J. Kubas and P. J. Vergamini, *Inorg. Chem.*, 1981, **20**, 2667.
17 P. J. Vergamini and G. J. Kubas, *Prog. Inorg. Chem.*, 1976, **21**, 261.
18 S. Dev, Y. Mizobe and M. Hidai, *Inorg. Chem.*, 1990, **29**, 4797.
19 U. Koelle, C. Rietmann and U. Englert, *J. Organomet. Chem.*, 1992, **423**, C20.
20 A. Hörnig, C. Rietmann, U. Englert, T. Wagner and U. Kölle, *Chem. Ber.*, 1993, **126**, 2609.
21 M. Hidai, Y. Mizobe and H. Matsuzaka, *J. Organomet. Chem.*, 1994, **473**, 1 and refs. therein.
22 H. Matsuzaka, Y. Takagi and M. Hidai, *Organometallics*, 1994, **13**, 13.
23 U. Koelle, C. Rietmann, J. Tjoe, T. Wagner and U. Englert, *Organometallics*, 1995, **14**, 703.
24 S. Kuwata, Y. Mizobe and M. Hidai, *Inorg. Chem.*, 1994, **33**, 3619.
25 F. Y. Pétillon, P. Schollhammer, J. Talarmin and K. W. Muir, *Coord. Chem. Rev.*, 1998, **178–180**, 203.
26 P. Schollhammer, F. Y. Pétillon, S. Poder-Guillou, J. Y. Saillard, J. Talarmin and K. W. Muir, *Chem. Commun.*, 1996, 2633; P. Schollhammer, E. Guénin, F. Y. Pétillon, J. Talarmin, K. W. Muir and D. S. Yufit, *Organometallics*, 1998, **17**, 1922.
27 J. F. Capon, P. Schollhammer, F. Y. Pétillon, J. Talarmin and K. W. Muir, unpublished work.
28 (*a*) M. Guéguen, F. Y. Pétillon and J. Talarmin, *Organometallics*, 1989, **8**, 148; (*b*) F. Y. Pétillon, S. Poder-Guillou, P. Schollhammer and J. Talarmin, *New J. Chem.*, 1997, **21**, 477.
29 F. Gloaguen, C. Le Floch, F. Y. Pétillon, J. Talarmin, M. El Khalifa and J. Y. Saillard, *Organometallics*, 1991, **10**, 2004.
30 S. D. Killops and S. A. R. Knox, *J. Chem. Soc., Dalton Trans.*, 1978, 1260.
31 H. S. Gutowski and C. H. Holm, *J. Chem. Phys.*, 1956, **25**, 1228.
32 H. Shanan-Atidi and K. H. Bar-Eli, *J. Chem. Phys.*, 1970, **74**, 961.
33 J. Sandström, in *Dynamic NMR Spectroscopy*, Academic Press, London, New York, 1982.
34 M. Guéguen, J. E. Guerchais, F. Y. Pétillon and J. Talarmin, *J. Chem. Soc., Chem. Commun.*, 1987, 557.
35 A. J. Bard and L. R. Faulkner, *Electrochemical Methods. Fundamentals and Applications*, Wiley, New York, 1980, ch. 11,

pp. 429–485; E. R. Brown and R. F. Large, in *Techniques of Chemistry*, ed. A. Weissberger, New York, Wiley, 1971, vol. 1, part IIA, ch. 6, pp. 423– 530.
36 R. S. Nicholson and I. Shain, *Anal. Chem.*, 1964, **36**, 706.
37 R. S. Nicholson, *Anal. Chem.*, 1966, **38**, 1406.
38 R. Hill, B. A. Kelly, F. G. Kennedy, S. A. R. Knox and P. Woodward, *J. Chem. Soc.*, *Chem. Commun.*, 1977, 434.
39 N. G. Connelly, G. A. Johnson, B. A. Kelly and P. Woodward, *J. Chem. Soc.*, *Chem. Commun.*, 1977, 436.
40 A. Takahashi, Y. Mizobe, H. Matsuzaka, S. Dev and M. Hidai, *J. Organomet. Chem.*, 1993, **456**, 243.
41 W. E. Geiger, P. H. Rieger, B. Tulyathan and M. D. Raush, *J. Am. Chem. Soc.*, 1984, **106**, 7000.
42 M. L. Abasq, D. L. Hughes, F. Y. Pétillon, R. Pichon, C. J. Pickett and J. Talarmin, *J. Chem. Soc.*, *Dalton Trans.*, 1997, 2279.
43 I. D. Benson, S. D. Killops, S. A. R. Knox and A. J. Welch, *J. Chem. Soc.*, *Chem. Commun.*, 1980, 1137.
44 R. D. Adams, D. F. Chodosh and E. Faraci, *Cryst. Struct. Comm.*, 1978, **7**, 145.
45 J. Courtot-Coupez, M. Guéguen, J. E. Guerchais, F. Y. Pétillon, J. Talarmin and R. Mercier, *J. Organomet. Chem.*, 1986, **312**, 81.
46 M. El Khalifa, F. Y. Pétillon, J. Y. Saillard and J. Talarmin, *Inorg. Chem.*, 1989, **28**, 3849.
47 S. Shaik, R. Hoffmann, C. R. Fisel and R. H. Summerville, *J. Am. Chem. Soc.*, 1980, **102**, 4555.
48 W. E. Geiger, *Prog. Inorg. Chem.*, 1985, **33**, 275.
49 D. H. Evans and K. M. O'Connell, in *Electroanalytical Chemistry*, ed. A. J. Bard, Marcel Dekker, New York, 1986, vol. 14, p. 113.
50 T. Gennett, W. E. Geiger, B. Willett and F. C. Anson, *J. Electroanal. Chem. Interfacial Electrochem.*, 1987, **222**, 151.
51 N. G. Connelly and L. F. Dahl, *J. Am. Chem. Soc.*, 1970, **92**, 7470.
52 M. El Khalifa, M. Guéguen, R. Mercier, F. Y. Pétillon, J. Y. Saillard and J. Talarmin, *Organometallics*, 1989, **8**, 140.
53 J. F. Capon, R. Kergoat, N. Le Berre-Cosquer, S. Péron, J. Y. Saillard and J. Talarmin, *Organometallics*, 1997, **16**, 4645.
54 R. Hoffmann and W. N. Lipscomb, *J. Chem. Phys.*, 1962, **36**, 2179; R. Hoffmann, *J. Chem. Phys.*, 1963, **39**, 1397.
55 J. M. Ammeter, H. B. Bürgi, J. C. Thibeault and R. Hoffmann, *J. Am. Chem. Soc.*, 1978, **100**, 3686.
56 S. Alvarez, Tables of Parameters for Extended Hückel Calculations, Departemento de Quimica Inorganica, University of Barcelona, 1989.
57 C. Mealli and D. Proserpio, *J. Chem. Educ.*, 1990, **67**, 399.
58 G. M. Sheldrick, SADABS, A program for empirical absorption correction, University of Göttingen, 1997.
59 G. M. Sheldrick, SHELXL 97, A program for the refinement of crystal structures, University of Göttingen, 1997.
60 L. J. Farrugia, WINGX, A program system for X-ray analysis, University of Glasgow, 1997.

Paper 9/02793I